Received: 11 October 2019 | Accepted: 12 February 2020

DOI: 10.1002/jcp.29653

ORIGINAL RESEARCH ARTICLE

Journal of Cellular Physiology WILEY

Loss and rescue of osteocalcin and osteopontin modulate osteogenic and angiogenic features of mesenchymal stem/stromal cells

Marta S. Carvalho[1,2] | João C. Silva[2,3] | Christopher M. Hoff[4] | Joaquim M. S. Cabral[2] | Robert J. Linhardt[1,3] | Cláudia L. da Silva[2] | Deepak Vashishth[1]

[1]Department of Biomedical Engineering, Center for Biotechnology and Interdisciplinary Studies, Rensselaer Polytechnic Institute, Troy, New York

[2]Department of Bioengineering and iBB – Institute for Bioengineering and Biosciences, Instituto Superior Técnico, Universidade de Lisboa, Lisboa, Portugal

[3]Department of Chemistry and Chemical Biology, Biological Sciences and Chemical and Biological Engineering, Center for Biotechnology and Interdisciplinary Studies, Rensselaer Polytechnic Institute, Troy, New York

[4]Department of Earth and Environmental Sciences, Rensselaer Polytechnic Institute, Troy, New York

Correspondence
Deepak Vashishth, PhD, Department of Biomedical Engineering, Center for Biotechnology and Interdisciplinary Studies, Rensselaer Polytechnic Institute, 110 8th Street, BT 2213, Troy, NY 12180-3590.
Email: vashid@rpi.edu

Funding information
Fundação para a Ciência e a Tecnologia, Grant/Award Numbers: SFRH/BD/105771/2014, SFRH/BD/52478/2014, UID/BIO/04565/2019; NIH, Grant/Award Number: AR49635

Abstract

Noncollagenous proteins in the bone extracellular matrix, such as osteocalcin (OC) and osteopontin (OPN), inherent to evolution of bone as a skeletal tissue, are known to regulate bone formation and mineralization. However, the fundamental basis of this regulatory role remains unknown. Here, for the first time, we use mouse mesenchymal stem/stromal cells (MSC) lacking both OC and OPN to investigate the mechanistic roles of OC and OPN on the proliferation capacity and differentiation ability of MSC. We found that the loss of OC and OPN reduces stem cells self-renewal potential and multipotency, affects their differentiation into an osteogenic lineage, and impairs their angiogenic potential while maintaining chondrogenic and adipogenic lineages. Moreover, loss of OC and OPN compromises the extracellular matrix integrity and maturation, observed by an unexpected enhancement of glycosaminoglycans content that are associated with a more primitive skeletal connective tissue, and by a delay on the maturation of mineral species produced. Interestingly, exogenously supplemented OC and OPN were able to rescue MSC proliferative and osteogenic potential along with matrix integrity and mineral quality. Taken together, these results highlight the key contributions of OC and OPN in enhancing osteogenesis and angiogenesis over primitive connective tissue, and support a potential therapeutic approach based on their exogenous supplementation.

KEYWORDS

angiogenesis, mesenchymal stem/stromal cells, osteocalcin, osteogenesis, osteopontin

1 | INTRODUCTION

Bone extracellular matrix (ECM) is composed of two components: mineral comprising mainly hydroxyapatite (HAP; 70–90%) and organic matrix (10–30%) comprising primarily collagen (approx. 90% of organic matrix), with the remaining component being noncollagenous proteins (~10%; Sroga, Karim, Colón, & Vashishth, 2011; Vashishth, 2007). Although noncollagenous proteins correspond to a small amount of the total protein mass of the bone ECM, these have been found to be biologically active and to modulate different functions in the bone, such as cell adhesion (Harris et al., 2000), cell differentiation (Ravindran & George, 2014), mineralization (Harris et al., 2000) and bone resorption/remodeling (Razzouk et al., 2002). Of these noncollagenous proteins, osteopontin (OPN) and osteocalcin (OC) are two of the most abundant, representing 10–20% of the noncollagenous proteins in bone tissue (Sroga, Karim, Colón, & Vashishth, 2011). OPN is an arginine–glycine–aspartate (RGD)-containing adhesive glycoprotein (Denhardt & Guo, 1993) and,

through its RGD domain, OPN can bind to $\alpha_v\beta_3$ integrins. In addition, OPN can also present a RGD-independent adhesion mechanism where it engages CD44 (Weber, Ashkar, Glimcher, & Cantor, 1996), a broadly distributed cell surface adhesion molecule involved in cell–cell and cell–matrix interactions. The precise function of OPN is still unknown, however, its ability to bind to several components suggests that OPN may have a multifaceted role in the regulation of several physiological processes, such as collagen organization, cell adhesion, cell viability, cell migration, angiogenesis, and calcification (Denhardt & Guo, 1993; Rodriguez et al., 2014; Sroga, Karim, Colón, & Vashishth, 2011). OC is the most abundant bone-specific non-collagenous protein in bone ECM and plays a crucial role in matrix mineralization, having affinity for calcium through its gama-carboxyglutamic acid residues (Ducy et al., 1996). OC also acts in cell signaling, in particular in bone resorption and deposition, by recruiting osteoclasts and osteoblasts, respectively (DeFranco, Glowacki, Cox, & Lian, 1991). Recently, new insights in the biology of OC have been extensively reviewed, suggesting a more complex role of OC in the regulation of whole body metabolism, besides matrix mineralization, influencing glucose metabolism, reproduction, and cognition (Zoch, Clemens, & Riddle, 2016).

Previous studies by our group and others have demonstrated the role of OPN and/or OC as structural molecules in bone matrix (Bailey, Karsenty, Gundberg & Vashishth, 2017; Morgan, Poundarik, & Vashishth, 2015; Nikel, Laurencin, McCallum, Gundberg, & Vashishth, 2013; Nikel, Poundarik, Bailey, & Vashishth, 2018; Sroga, Karim, Colón, & Vashishth, 2011), linking the organic and inorganic matrices by forming a tether between collagen fibrils and mineral crystals (Poundarik et al., 2012). In fact, both OC and OPN have specific roles in the biomolecular regulation of mineral in bone, being important to determine the quality of bone mineral (Poundarik, Boskey, Gundberg, & Vashishth, 2018). Moreover, loss and modification of OC and/or OPN from bone matrix known to occur with tissue age (Sroga, Karim, Colón, & Vashishth, 2011) and with aging in humans (Boskey & Coleman, 2010; Ingram, Park, Clarke, & Fitzpatrick, 1994), explain loss of structural integrity (Poundarik et al., 2012; Sroga & Vashishth, 2018) and altered mineralization (Boskey, Maresca, & Appel, 1989; Rodriguez et al., 2014).

Moreover, bone tissue contains less than 1% of glycosaminoglycans (GAG; Mania et al., 2009), which consist of ~90% chondroitin-4-sulfate (C4S) and small amounts of hyaluronic acid (HA), chondroitin-6-sulfate (C6S), and heparin sulfate (HS; Prince & Navia, 1983). In fact, changes in GAG composition of bone matrix may help to understand the mineralization process. Furthermore, abnormal expression of proteoglycans under bone pathologic conditions has also been suggested to result in modulation of bone mineralization (Theocharis et al., 2006).

HAP, $Ca_{10}(PO_4)_6(OH)_2$, is the major mineral component of bone tissue and can be found within the extracellular matrices of collagen fibers, as well as embedded within the noncollagenous proteins. HAP distribution has shown to increase with maturation of bone tissue and, thus, previous studies have used it as a marker to assess osteogenic differentiation of mesenchymal stem/stromal cells (MSC; Tsao et al., 2017). However, besides HAP, different mineral species can be found in bone, such as amorphous calcium phosphate (ACP), octacalcium phosphate (OCP), β-tricalcium phosphate (β-TCP), and dicalcium phosphate dihydrate (Boskey, 1992). Different techniques, such as Raman and Fourier-transform infrared (FTIR) spectroscopy (Egusa et al., 2014; Hung, Kuo, Chen, Chiang, & Lee, 2013; Tsao et al., 2017) have been applied to detect these mineral species during mineralization and, with the emergence of novel advanced tools, these can now be expanded to understand maturation and temporal regulation of mineralization and to distinguish different mineral species, including HAP, OCP, and β-TCP produced by osteoblasts derived from nonmodified/modified cell lines.

At the cellular level, it has been suggested that alterations in the levels of OPN or OC in stem cell culture, by genetic ablation or antibody neutralization, may have a negative effect on mineralization possibly due to impaired osteogenic differentiation of MSC (Chen et al., 2014). In vivo studies have also reported the delayed bone formation capacity of $OPN^{-/-}$ MSC. Moreover, some studies have demonstrated that OC modulates the mineral maturation during osteogenic differentiation of MSC (Tsao et al., 2017). Given that OC and OPN are inherently associated with evolution of bone and calcified cartilage (Laizé, Martel, Viegas, Price, & Cancela, 2005; Gómez-Picos, 2015), the loss of OPN and OC may have a broad impact on MSC and the resulting tissue, however, no information is currently available.

In this study, we isolated bone marrow–derived MSC from wild type (WT) and $OC^{-/-}$ $OPN^{-/-}$ mice and examined the combined role of OC and OPN on MSC proliferation, multilineage differentiation (adipogenic, chondrogenic, and osteogenic), angiogenic potential, and in the regulation of ECM. Moreover, using spectroscopic analysis, we assessed the maturation level of mineral species produced by differentiated $OC^{-/-}$ $OPN^{-/-}$ MSC. Next, to establish causality between the loss of OC and OPN expression and the impaired cell features, we evaluated whether exogenous supplementation of OC and OPN rescues/improves mineralization in $OC^{-/-}$ $OPN^{-/-}$ MSC cultures.

2 | MATERIALS AND METHODS

2.1 | Isolation of bone marrow–derived MSC

$OC^{-/-}$ $OPN^{-/-}$ mutant mice and C57BL/6 WT littermate mice ($n = 3$) were obtained from Prof. Caren Gundberg (Department of Orthopedics and Rehabilitation, Yale; Bailey et al., 2017; Poundarik, Boskey, Gundberg, & Vashishth, 2018; Poundarik et al., 2012). The $OC^{-/-}$ $OPN^{-/-}$ genotype was generated by breeding $OC^{-/-}$ mice with $OPN^{-/-}$ mice. All procedures were approved by the Institutional Animal Care and Use Committee (IACUC) of Rensselaer Polytechnic Institute.

Mice aged 8 months were killed and femur and tibia were collected. MSC were isolated from the bone marrow according to previous protocols (Nadri et al., 2007). In brief, the bone marrow was flushed into a tube and the solution was triturated extensively. Then,

the solution was carefully added onto Ficoll (GE Healthcare, Chicago, IL) and centrifuged at 400 rcf for 40 min. After that, the top layer was discarded and the second layer was collected. Upon subsequent washes, low-glucose Dulbecco's modified Eagle's medium (DMEM; Gibco, Grand Island, NY), supplemented with 15% fetal bovine serum (FBS; Gibco) and 1% penicillin-streptomycin (Pen-strep: Gibco; DMEM + 15% FBS) was added to the cell pellet and transferred to a T-75 cm^2 flask and kept at 37°C, 5% O_2, 5% CO_2 in a humidified atmosphere. Nonadherent cells were removed after 72 hr. The medium was changed every 3–4 days. After confluence, the cells were cryopreserved in liquid/vapor-phase nitrogen.

2.2 | Cell culture

Bone marrow–derived MSC from WT and $OC^{-/-}$ $OPN^{-/-}$ mice were thawed and plated on T-75 cm^2 flasks using DMEM + 15% FBS (Gibco) and kept at 37°C, 5% O_2 and 5% CO_2 in a humidified atmosphere. The medium renewal was performed every 3–4 days. The cells between passages 2 and 9 were used. Human umbilical vein endothelial cells (HUVEC) were purchased from Lonza (Basel, Switzerland) and maintained in commercial Endothelial Growth Medium-2 (EGM-2; Lonza) at 37°C, 21% O_2 and 5% CO_2 in a humidified atmosphere.

2.3 | Flow cytometric analysis

The cells were harvested, washed with the staining buffer, and suspended in the staining buffer at a concentration of 1×10^7 cells/ml. Then, 100 µl of cell suspension was incubated for 45 min at room temperature in the dark with each antibody (CD29, CD105, Sca-1, CD45) or with the corresponding isotype control antibody (R&D Systems, Minneapolis, MN). Following the incubation, excess antibody was removed by washing the cells with the staining buffer. Flow cytometric analysis was performed using LSR II flow cytometer (BD Biosciences, San Jose, CA). BD FACSDiva™ software was used for data analysis.

2.4 | Cell morphology

$OC^{-/-}$ $OPN^{-/-}$ and WT MSC were seeded onto 24-well plates and cell morphology was assessed after 24 hr and 4 days of culture. The cells were washed twice with phosphate-buffered saline (PBS; Gibco), fixed with 4% paraformaldehyde (PFA; Santa Cruz Biotechnology, Dallas, TX) for 20 min, and then permeabilized with 0.1% Triton X-100 (Sigma-Aldrich, St. Louis, MO) for 10 min. After permeabilization, the cells were incubated with phalloidin-TRITC (Sigma-Aldrich; dilution 1:250, 2 µg/ml) for 45 min in the dark. Then, the cells were washed twice with PBS and counterstained with 4′,6-diamidino-2-phenylindole (DAPI; Sigma-Aldrich; 1.5 µg/ml) for 5 min and washed with PBS. The cells were imaged by fluorescence microscope (Olympus IX51 Inverted Microscope; Olympus America Inc., Melville, NY).

2.5 | Proliferation assays

$OC^{-/-}$ $OPN^{-/-}$ and WT MSC were expanded during nine consecutive passages. The cells were plated into 12-well plates at two different seeding densities: 3,000 cells/cm^2 and 10,000 cells/cm^2 using DMEM + 15% FBS as growth medium. After reaching 80% confluence, the cells were harvested using TrypLE™ solution (Gibco) and plated into a different well. Fold increase and cumulative population doublings were calculated for each cell type at both cell densities. A kinetic study was performed in 12-well plate at a density of 5,000 cells/cm^2 per well in triplicate. After days 1, 4, 7, 12, and 15, the cells from $OC^{-/-}$ $OPN^{-/-}$ and WT were harvested and counted to calculate cell growth curves.

2.6 | Multilineage differentiation assays

To verify multipotency of mouse MSC, an in vitro differentiation assay kit from R&D Systems was used (mouse mesenchymal stem cell functional identification kit). MSC were grown in 24-well plates with medium changes every 3–4 days. For adipogenic differentiation, MSC were cultured in DMEM + 10% FBS + 1% Pen-strep (Gibco) with adipogenic supplement containing hydrocortisone, isobutylmethylxanthine and indomethacin (adipogenic differentiation medium; R&D Systems). The presence of adipocytes was verified by staining for triglycerides with Oil Red O (Sigma-Aldrich), an indicator of intracellular lipids accumulation. For osteogenic differentiation, MSC were cultured in DMEM + 10% FBS + 1% Pen-strep (Gibco) with osteogenic supplement containing dexamethasone, ascorbic acid, β-glycerophosphate (osteogenic differentiation medium; R&D Systems). These cultures were then stained with alkaline phosphatase (ALP) and Von Kossa stainings to identify ALP activity and calcium deposition, respectively, indicating active osteoblasts. For chondrogenic differentiation, MSC were transferred to a conical tube and chondrogenic differentiation medium was added, containing dexamethasone, ascorbate-phosphate, proline, pyruvate, recombinant human TGF-β3, and ITS supplement (insulin, transferrin, selenious acid, bovine serum albumin (BSA), and linoleic acid; chondrogenic differentiation medium, R&D Systems). These cultures were stained with Alcian Blue (Sigma-Aldrich).

For histological staining, the cells were fixed with 4% of PFA for 20 min. Then, the cells were rinsed in miliQ water for 15 min and incubated with different reagents, such as Oil Red O for adipogenic differentiation and with Alcian Blue for chondrogenic differentiation. For osteogenic differentiation, the cells were incubated with a Fast Violet solution (Sigma-Aldrich) and Naphthol AS-MX phosphate alkaline solution (Sigma-Aldrich) in a final concentration of 4% for 45 min, at room temperature in the dark. The cells were, then, washed three times with miliQ water and once with PBS. Von Kossa staining was then performed by incubating the cells with a 2.5%

silver nitrate solution (Sigma-Aldrich) for 30 min at room temperature in the dark. The cells were then washed three times with miliQ water and imaged (Olympus IX51 Inverted Microscope). To visualize the mineral deposits formed in the cell culture after osteogenic differentiation, a 20 mM xylenol orange (XO) solution (Sigma-Aldrich) was added to the previously fixed cells and incubated for 1 hr at room temperature in the dark. After that, the cells were washed with miliQ water and the cell nuclei were counterstained with DAPI (Sigma-Aldrich; 1.5 μg/ml) for 5 min and washed with PBS. Following staining, fluorescent microscopy was used to image the resulting mineral deposits (Olympus IX51 Inverted Microscope).

2.7 | Immunofluorescent staining

MSC were plated in 24-well plates and adipogenic, chondrogenic, and osteogenic differentiations were induced. At different timepoints of differentiation, the cells were washed with PBS and fixed with 4% PFA for 20 min at room temperature. The cells were then washed three times with 1% BSA (Sigma-Aldrich) in PBS for 5 min, permeabilized and blocked with a solution of 0.3% Triton X-100, 1% BSA, and 10% donkey serum in PBS at room temperature for 45 min. Primary antibodies including goat anti-mouse FABP4, sheep anti-mouse collagen II, and goat anti-mouse OPN (10 μg/ml in 0.3% Triton X-100, 1% BSA, 10% donkey serum; R&D Systems) were added followed by overnight incubation at 4°C. After washing with 1% BSA in PBS, NorthernLights™ 557-conjugated anti-goat and anti-sheep IgG secondary antibody (dilution 1:200 in 1% BSA/PBS; R&D Systems) were added into the samples and incubated in the dark for 1 hr at room temperature. Finally, the cell nuclei were counterstained with DAPI (Sigma-Aldrich; 1.5 μg/ml) for 5 min and then washed with PBS. The fluorescent staining was imaged by fluorescence microscope (Olympus IX51 Inverted Microscope).

2.8 | Calcium quantification assay

For determination of total calcium content, the samples ($n = 3$) were washed twice with PBS and extracted in 0.5 M HCl solution (Sigma-Aldrich). Accumulated calcium was removed from the cellular component by shaking overnight at 4°C. The consequent supernatant was used for calcium determination according to the manufacturer's instructions contained in the calcium colorimetric assay kit (Stanbio Laboratory, Boerne, TX). Absorbance at 550 nm was measured for each condition and normalized to the total number of cells, after 7, 15, and 21 days of osteogenic differentiation.

2.9 | Alkaline phosphatase activity

ALP activity was detected using a colorimetric ALP kit (BioAssays Systems, Hayward, CA) according to the manufacturer's protocol. The samples ($n = 3$) were washed with PBS and incubated in the lysis buffer (0.1% Triton X-100 in PBS) by shaking for 30 min at room temperature. The lysate was added to *p*-nitrophenyl phosphate solution (10 mM) provided with the ALP kit. The absorbance was measured at 405 nm and normalized to the total number of cells in each sample, after 7, 15, and 21 days of osteogenic differentiation.

2.10 | Exogenous supplementation of OC/OPN on MSC culture

To evaluate if exogenous supplementation of OC and OPN could rescue the proliferative and osteogenic potential of $OC^{-/-}$ $OPN^{-/-}$ MSC, OC fragment 1-49 (Sigma-Aldrich) and/or recombinant OPN (R&D Systems) were added into the culture medium (1 μg/ml). Proliferation of $OC^{-/-}$ $OPN^{-/-}$ MSC was assessed by supplementing the growth medium (DMEM + 15%FBS + 1% Pen/strep) with OC and/or OPN (1 μg/ml OC and/or OPN). To assess osteogenic potential, $OC^{-/-}$ $OPN^{-/-}$ MSC were cultured under osteogenic differentiation medium supplemented with OC and OPN (1 μg/ml each protein). The medium was changed every 3–4 days and OC/OPN were added into the system in each medium renewal.

2.11 | In vitro endothelial cell tube formation assay

To study the role of OC and OPN on the angiogenic features of MSC, a tube formation assay was performed. Red fluorescent protein (RFP)-tagged HUVEC (2×10^4 cells) were cultured on a Matrigel substrate (50 μl per well; Corning, Corning, NY) in a 96-well plate, incubated with conditioned medium (CM) from WT and $OC^{-/-}$ $OPN^{-/-}$ MSC. This conditioned medium was collected after 72 hr in basal DMEM (without FBS; 37°C, 5% O_2, 5% CO_2). HUVEC were also incubated with EGM-2 (Lonza), as a positive control, whereas basal DMEM was used as a negative control. After incubation for 8 hr at 37°C, three photomicrographs per well were taken (Olympus IX51 Inverted Microscope) and the number of tubes formed was determined using ImageJ (NIH) software.

In a different assay, $OC^{-/-}$ $OPN^{-/-}$ and WT MSC were cocultured with RFP-tagged HUVEC (1:1, 2×10^4 cells) on a Matrigel substrate using EGM-2 and HUVEC distribution was evaluated. In addition, the cocultures between HUVEC and $OC^{-/-}$ $OPN^{-/-}$ were cultured on a Matrigel substrate with EGM-2 supplemented with OC fragment 149 (Sigma-Aldrich) and/or recombinant OPN (R&D Systems; 1 μg/ml each protein) and with recombinant vascular endothelial growth factor (VEGF; R&D Systems; 50 ng/ml) to analyze if HUVEC were able to rescue their tube formation capability. After 8 hr of incubation at 37°C, the micrographs were taken under fluorescence microscope (Olympus IX51 Inverted Microscope) and the number of tubes formed was counted using ImageJ (NIH) software.

2.12 | Cell migration assay

The 24-well tissue culture plates were collagen-coated by incubation in 0.2 mg/ml of collagen type I solution (Sigma-Aldrich) for 2 hr at

37°C before rinsing with PBS. Each well was seeded with HUVEC at 10,000 cells/cm^2 and maintained at 37°C, 21% O_2 and 5% CO_2 conditions for 48 hr to allow cell adhesion and the formation of a confluent monolayer. These confluent monolayers were then scratched with a sterile pipette tip, creating a scratch (wound) of approximately 0.25–0.3 mm in width. After creating the scratch, the culture medium was then removed and replaced with conditioned medium, which had been generated from WT and OC$^{-/-}$OPN$^{-/-}$ MSC cultured for 72 hr using basal DMEM medium without FBS (37°C, 5% O_2, 5% CO_2). HUVEC migration was monitored by image collection at various time intervals (0, 4, 8, 10, and 12 hr) after the scratch was performed. The migration distance was quantified with the use of ImageJ (NIH) software, measuring the width of the scratch at previously defined points along its length (top, middle, and bottom of the field of view). Data has been presented as extent of the cell migration, that is, the percentage by which HUVEC migrate for each given time point compared with the original scratch width.

2.13 | Quantitative reverse transcription polymerase chain reaction (qRT-PCR) analysis

Total RNA was extracted using the RNeasy Mini Kit (Qiagen, Hilden, Germany). cDNA was synthesized from 20 ng of total RNA using iScript™ Reverse Transcription Supermix (Bio-Rad, Hercules, CA). Reaction mixtures (20 μl) were incubated in a thermal cycler for 5 min at 25°C, 30 min at 42°C, and 5 min at 85°C and then maintained at 4°C. The sequences of the specific primer sets used are given in Table 1.

The qRT-PCR was performed using PowerUp SYBR Green Master Mix (Applied Biosystems, Foster, CA) and StepOnePlus real-time PCR system (Applied Biosystems). All reactions were carried out at 95°C for 10 min, followed by 40 cycles of 95°C for 15 s and 60°C for 1 min and all were performed in triplicate. β-Actin was used as an endogenous control. A threshold cycle (C_t) was observed in the exponential phase of amplification and quantification of relative expression levels was performed with the use of standard curves for target genes and endogenous control. Geometric means were used to calculate the $\Delta\Delta C_t$ values and expressed as 2-$\Delta\Delta C_t$. The mean values from triplicate analysis were compared. The value of WT control samples (undifferentiated cells) was set as 1 and used as reference to calculate the fold-change differences in each target gene.

TABLE 1 Sequences of primers used for qRT-PCR analysis

Genes	Sequences
β-Actin	For: 5′ TTC CAG CCT TCC TTC TTG GG Rev: 5′ TGT TGG CAT AGA GGT CTT TTA CGG
Col I	For:5′ GCT CCT CTT AGG GGC CAC T Rev: 5′ CCA CGT CTC ACC ATT GGG G
Runx2	For: 5′ CCA CGG CCC TCC CTG AAC TCT Rev: 5′ ACT GGC GGG GTG TAG GTA AAG GTG
ALP	For: 5′ CCA ACT CTT TTG TGC CAG AGA Rev: 5′ GGC TAC ATT GGT GTT GAG CTT TT
OPN	For: 5′ AGC AAG AAA CTC TTC CAA GCA A Rev: 5′ GTG AGA TTC GTC AGA TTC ATC CG
OC	For: 5′ GCC CTG AGT CTG ACA AAG GTA Rev: 5′ GGT GAT GGC CAA GAC TAA GG

2.14 | Scanning electron microscopy and elemental analysis

The morphological and structural characterization of MSC was performed using a field emission scanning electron microscope (FE-SEM; FEI-Versa 3D Dual Beam, Hillsboro). The elemental analysis of MSC after osteogenic differentiation was performed using a scanning electron microscope attached with an energy dispersive electron probe X-ray analyzer (SEM-EDS; Carl Zeiss ultra 1540 dual beam FIB/SEM system). Before imaging, the samples were dehydrated by a graded series of ethanol and dried in a critical CO_2 point dryer (Supercritical Automegasamdri 915B, Tousimis). Afterward, the samples were mounted on a holder and sputter-coated with a thin layer of 60% gold-40% palladium. The samples were imaged at several magnifications using an accelerating voltage of 2–3 kV.

2.15 | Raman and FTIR spectroscopy

For sample preparation, MSC were harvested at different timepoints and washed twice with dH_2O. After that, the cells were kept at −80°C and were then freeze-dried. The lyophilized samples were used for Raman and FTIR analysis.

Attenuated total reflectance-Fourier-transform infrared (ATR-FTIR) spectra of lyophilized minerals from the cell cultures were collected with a VERTEX 70 FT-IR spectrometer (Bruker, Billerica, MA) with a Hyperion infrared microscope, using an mercury cadmium telluride detector and a germanium ATR objective.

Raman microscope (Senterra Raman microscope, Bruker) was used as the setup of Raman spectroscopy. A 100 mW laser operating at 785 nm was used to provide the Raman excitation light source. The objective lens of ×20 was used. Raman signals were collected from the spectrum between 600 and 1800 cm^{-1} with an integration time of 20 s. Raman spectra were obtained from at least three locations selected from each sample. Three independent samples were performed. Multipoint baseline correction by OPUS software (Bruker) was used.

2.16 | GAG disaccharide sample preparation: isolation, digestion, and AMAC-labeling

The cells (WT and OC$^{-/-}$ OPN$^{-/-}$ MSC; 100,000 cells per sample) were treated with the BugBuster 10X Protein Extraction Reagent (Millipore Sigma, MA) and sonicated for 1 hr. The samples were then desalted by passing through a 3 kDa molecular weight cut off spin

column (Millipore, MA) and washed three times with distilled water. The 300 μl of digestion buffer (50 mM ammonium acetate containing 2 mM calcium chloride adjusted to pH 7.0) was added to the filter unit. Recombinant heparin lyases I, II, III (10 mU each, pH optima 7.0–7.5) and recombinant chondroitin lyase ABC (10 mU each, pH optimum 7.4) were added to each sample and incubated overnight at 37°C to enable GAG enzymatic digestion. Afterward, the enzymatic reaction was terminated by ultracentrifugation and the filter unit was washed twice with 200 μl of distilled water. The final filtrates containing the disaccharide products were lyophilized and kept at −20°C until labeling. The samples were AMAC-labeled by adding 10 μl of 0.1 M AMAC in dimethyl sulfoxide/acetic acid (17/3, vol/vol) solution. Then, the samples were incubated at room temperature for 10 min, followed by addition of 10 μl of 1 M aqueous $NaCNBH_4$ solution and incubation for 1 hr at 45°C. A mixture containing all 17 CS, HS, and HA disaccharide standards (0.5 ng/μl) was also AMAC-labeled and used for each run as an external standard. After the AMAC-labeling reaction, the samples were centrifuged and supernatants recovered.

2.17 | Compositional analysis of GAG disaccharides by LC-MS/MS

The disaccharide analysis was performed according to a previous protocol (Silva et al., 2019; Sun et al., 2015). LC was performed on an Agilent 1200 LC system at 45°C using an Agilent Poroshell 120 ECC18 (2.7 μm, 3.0 × 50 mm) column. Mobile phase A was 50 mM ammonium acetate aqueous solution and the mobile phase B was methanol. The mobile phase passed through the column at a flow rate of 300 μl/min. The gradient used was the following: 0–10 min, 5–45% B; 10–10.2 min, 45–100% B; 10.2–14 min, 100% B; 14–22 min, 100–5% B. The injection volume used for all the samples was 5 μl. A triple quadrupole mass spectrometry system equipped with an ESI source (Thermo Fisher Scientific, San Jose, CA) was used as a detector. The online MS analysis was performed at the multiple reaction monitoring (MRM) mode with the MS parameters: negative ionization mode with a spray voltage of 3000 V, a vaporizer temperature of 300°C, and a capillary temperature of 270°C. Data analysis was performed using Thermo Xcalibur™ software (Thermo Fisher Scientific). The disaccharides in different cell samples were quantified by comparing the sample peak area to an external standard.

2.18 | Statistical analysis

Each experiment was conducted in triplicate. Statistical analysis of the data was performed using Student's *t* test, comparing each condition with the WT control groups at the same time point, using GraphPad Prism version 7. The statistical significance of results is reported at 95% confidence intervals ($p < .05$).

3 | RESULTS

3.1 | Bone marrow–derived MSC isolation and characterization

The morphology of MSC isolated from bone marrow of WT and OC/OPN double knockout (KO) mice was similar, however, we could observe that, after 4 days of cell culture, WT MSC proliferated much more than $OC^{-/-}$ $OPN^{-/-}$ MSC, as higher numbers of WT MSC were observed compared with $OC^{-/-}OPN^{-/-}$ MSC (Figure 1). The expression of surface markers such as CD105, CD29, and Sca-1 was confirmed by flow cytometry, as well as the absence of expression of the surface marker CD45 for MSC isolated from both WT and $OC^{-/-}$ $OPN^{-/-}$ mice, confirming the successful isolation of MSC from both groups (Figure S1A). The downregulation of OC and OPN osteogenic genes was also confirmed by qRT-PCR for $OC^{-/-}$ $OPN^{-/-}$ MSC (Figure S1B).

3.2 | Loss of OC and OPN impairs the proliferative capacity of MSC

$OC^{-/-}$ $OPN^{-/-}$ MSC cultured at 3,000 cells/cm^2 (low density) took 71 days to complete nine passages, while WT MSC took only 48 days (Figure S2). When cultured at a higher density (10,000 cells/cm^2), $OC^{-/-}$ $OPN^{-/-}$ MSC reached nine passages after 49 days, while WT MSC only took 34 days (Figure S2D). At the end of the ninth passage, cumulative population doublings of 9.96 ± 0.78 and 16.18 ± 0.52 were obtained for WT MSC cultured at 10,000 cells/cm^2 and 3,000 cells/cm^2, respectively (Figure S2B, 2D). On the other hand, at the end of the ninth passage, $OC^{-/-}$ $OPN^{-/-}$ MSC only achieved cumulative population doublings of 6.17 ± 0.14 and 7.57 ± 0.1, when cultured at 10,000 cells/cm^2 and 3,000 cells/cm^2, respectively (Figure S2B, 2D). Interestingly, the proliferative potential of $OC^{-/-}$ $OPN^{-/-}$ MSC was always affected, even when two different cell seeding densities were investigated, reaching cumulative population doublings very similar for both cell seeding densities. Kinetic study showed that $OC^{-/-}$ $OPN^{-/-}$ MSC proliferated slower than WT MSC. Interestingly, only after 7 days in culture, $OC^{-/-}$ $OPN^{-/-}$ MSC started to proliferate faster, reaching higher cell numbers. After 15 days in culture, WT MSC presented a statistically significant increase in proliferation, reaching a cell number of (5.42 ± 0.47) $x10^4$, whereas $OC^{-/-}$ $OPN^{-/-}$ MSC achieved (4.39 ± 0.38) $x10^4$ cells (Figure 1c). Taken together, these results show that lack of OC and OPN delays the proliferation of MSC in vitro.

3.3 | Loss of OC and OPN maintains stem cell multipotency but impairs osteogenic differentiation

Following treatment with adipogenic differentiation medium, $OC^{-/-}$ $OPN^{-/-}$ MSC changed to express Oil Red O-stained vesicles, showing that these successfully differentiated into adipose cells,

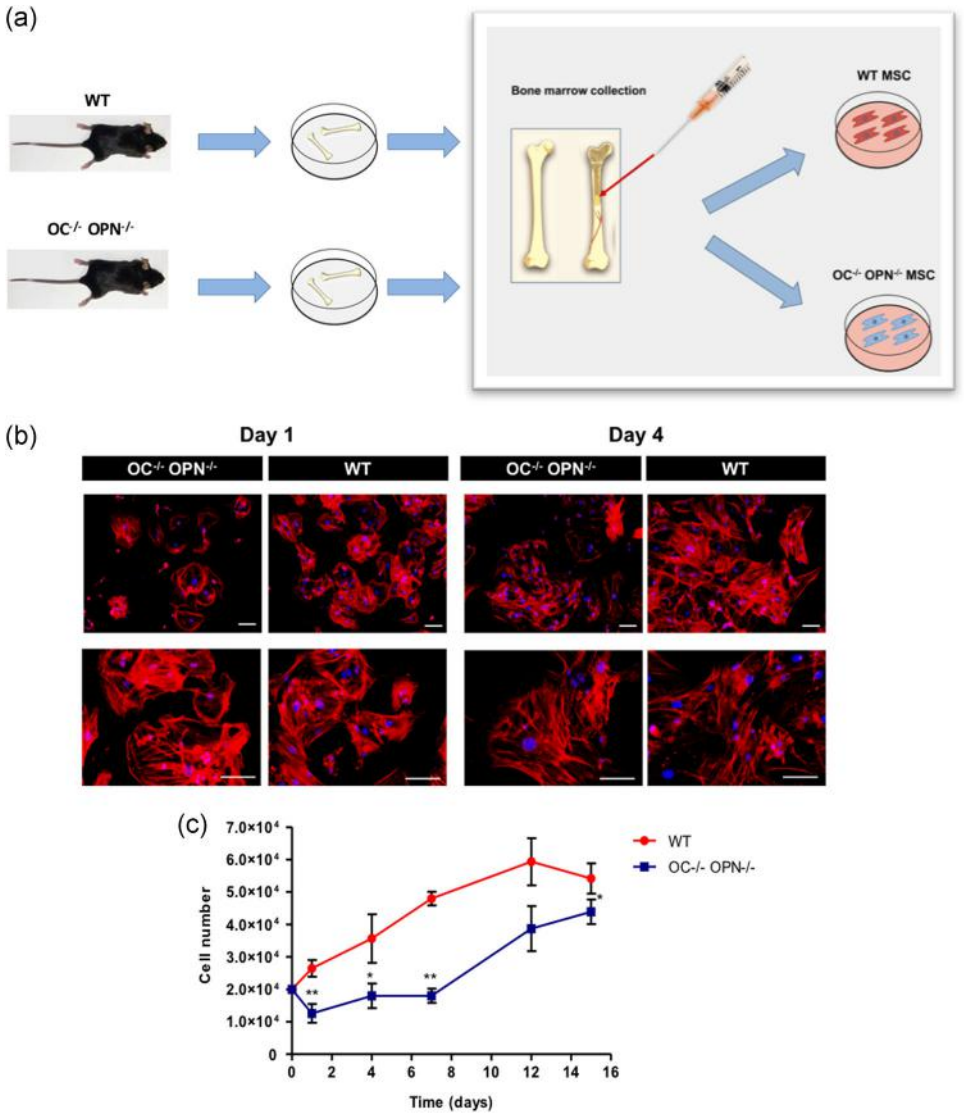

FIGURE 1 Bone marrow–derived MSC isolation and characterization. (a) Schematics of bone marrow MSC isolation from femur and tibia of $OC^{-/-}$ $OPN^{-/-}$ and WT mice. (b) Cell morphology after 24 hr and 4 days of culture. Red: phalloidin, blue: DAPI. Scale bar = 100 μm. (c) Kinetic study during 15 days of cell culture. Data are expressed as mean ± *SD*. DAPI, 4′,6-diamidino-2-phenylindole; MSC, mesenchymal stem/stromal cells; OC, osteocalcin; OPN, osteopontin; WT, wild type. $^{**}p < .01$; $^{*}p < .05$

like WT MSC (Figure 2a). The expression of FABP4 was also confirmed by immunocytochemistry (Figure S3A). Furthermore, after chondrogenic induction, the cells changed to show deposition of ECM in the pellet culture, stained with Alcian Blue (Figure 2a). Collagen type II, a biomarker of chondrocytes, was also detected for both cell types, WT and $OC^{-/-}$ $OPN^{-/-}$ MSC (Figure S3B). Regarding the osteogenic lineage, $OC^{-/-}$ $OPN^{-/-}$ MSC demonstrated an impaired or incomplete differentiation profile compared with WT MSC under the same conditions. Although $OC^{-/-}$ $OPN^{-/-}$ MSC underwent osteogenic commitment and presented similar ALP activity to WT MSC, limited increase in calcium deposits in the matrix produced by $OC^{-/-}$ $OPN^{-/-}$ MSC, after 21 days of osteogenic differentiation, was observed by Von Kossa and Xylenol Orange stainings (Figure 2a,d,e). As expected, immunocytochemistry confirmed that $OC^{-/-}$ $OPN^{-/-}$ MSC did not express OPN (Figure S3C).

Quantification of calcium deposition demonstrated that the kinetics of osteogenic differentiation by $OC^{-/-}$ $OPN^{-/-}$ MSC was significantly altered compared with WT MSC (Figure 2c). For example, after 15 days of differentiation, an increase of calcium deposition was observed only for WT MSC. In addition, calcium quantification demonstrated that $OC^{-/-}$ $OPN^{-/-}$ MSC produced smaller amount of mineral after 21 days of differentiation, compared with WT MSC. These results were further confirmed with Xylenol Orange staining, indicating a smaller extent of mineralization for $OC^{-/-}$ $OPN^{-/-}$ MSC (Figure 2d,e).

SEM micrographs of $OC^{-/-}$ $OPN^{-/-}$ and WT MSC demonstrated a higher amount of mineralized nodules produced in the WT MSC after

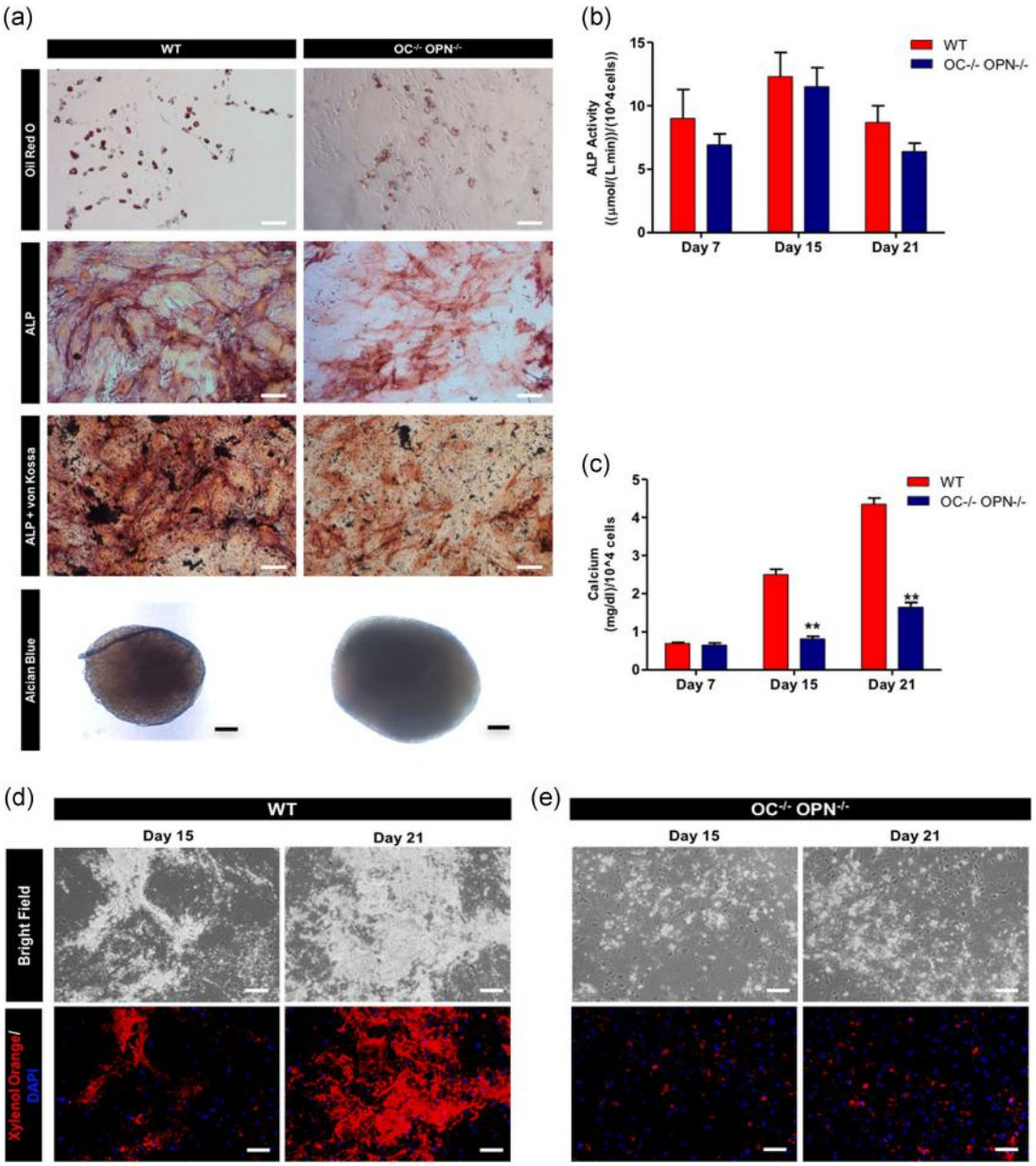

FIGURE 2 OC/OPN deficiency impairs MSC osteogenic differentiation. (a) WT and $OC^{-/-}$ $OPN^{-/-}$ MSC were cultured in adipogenic (7 days), osteogenic, and chondrogenic differentiation medium (21 days) and stained with Oil Red O to reveal lipid droplets, ALP and Von Kossa stainings to detect mineralization and Alcian Blue to detect glycosaminoglycans. (b) ALP activity was evaluated after 7, 15, and 21 days of osteogenic differentiation. (c) Calcium deposits were quantified after 7, 15, and 21 days of osteogenic differentiation. (d, e) MSC from WT (d) and $OC^{-/-}$ $OPN^{-/-}$ (e) were cultured in osteogenic differentiation medium for the indicated number of days and calcium deposits were revealed by Xylenol Orange stain (red) (blue: DAPI). Scale bar = 100 µm. Values are means ± *SD*. ALP, alkaline phosphatase; DAPI, 4′,6-diamidino-2-phenylindole; MSC, mesenchymal stem/stromal cells; OC, osteocalcin; OPN, osteopontin; WT, wild type. $^{**}p < .01$

15 and 21 days of osteogenic differentiation (Figure S4A). However, elemental analysis of both cell types, after 21 days of osteogenic differentiation, demonstrated the presence of the same components, presenting calcium and phosphorous in their composition (Figure S4B, 4C). Interestingly, after 30 days of osteogenic differentiation, WT MSC and $OC^{-/-}$ $OPN^{-/-}$ MSC showed the same morphology presenting mineralized nodules.

Gene expression analysis at different timepoints showed that $OC^{-/-}$ $OPN^{-/-}$ MSC downregulated selected osteogenic genes compared with WT MSC (Figure 3). *Runx2* gene expression was impaired by the lack of OC and OPN during the 21 days of osteogenic differentiation. Although a slight increase was observed in *Col I* gene expression after 21 days of differentiation for both cell types, the relative expression of *Col I* from $OC^{-/-}$ $OPN^{-/-}$ was significantly lower than WT MSC. WT MSC upregulated the expression of *OPN* and *OC* genes during osteogenic differentiation, however, as expected, $OC^{-/-}$ $OPN^{-/-}$ MSC did not demonstrate expression of these genes. In contrast, *ALP* gene expression level

was enhanced in $OC^{-/-}$ $OPN^{-/-}$ MSC compared with WT MSC. Interestingly, the expression of *ALP* gene was enhanced after 7 and 15 days of differentiation but it decreased after 21 days for both cell types, reaching its peak after 15 days of osteogenic differentiation for both cell types.

3.4 | Loss of OC and OPN compromises matrix integrity and maturation level of mineral species produced by MSC

After 21 days under osteogenic culture conditions, FTIR spectra of the sample produced by WT MSC became similar to the typical infrared vibrations of phosphate, carbonate, and amide I and II. The presence of crystalline apatite was verified by a split phosphate band 500–635 cm^{-1}; Figure 4a). In contrast, the sample produced by $OC^{-/-}$ $OPN^{-/-}$ MSC did not demonstrate the absorption peaks associated with major bone-related molecular species. Moreover, the spectrum generated by $OC^{-/-}$ $OPN^{-/-}$ MSC, after 21 days of osteogenic differentiation, was similar to the spectra of WT and $OC^{-/-}$ $OPN^{-/-}$ MSC before differentiation (Figure 4a). This result confirmed that the absence of OC and OPN impairs the mineralization capacity of cultured MSC.

To elucidate the differential production of mineralized matrix during osteogenic differentiation of MSC, Raman spectra were recorded on days 0, 15, 21, and 30. The region of Raman spectra of cellular components is marked in gray, and the region of mineral species is marked in yellow (Figure S5). Peaks related to cellular components, such as phenylalanine (1,003 cm^{-1}), CH_2 wag (1,449 cm^{-1}) and amide I (1,660 cm^{-1}), were present in Raman spectra from both $OC^{-/-}$ $OPN^{-/-}$ and WT MSC (Figure S5). Raman

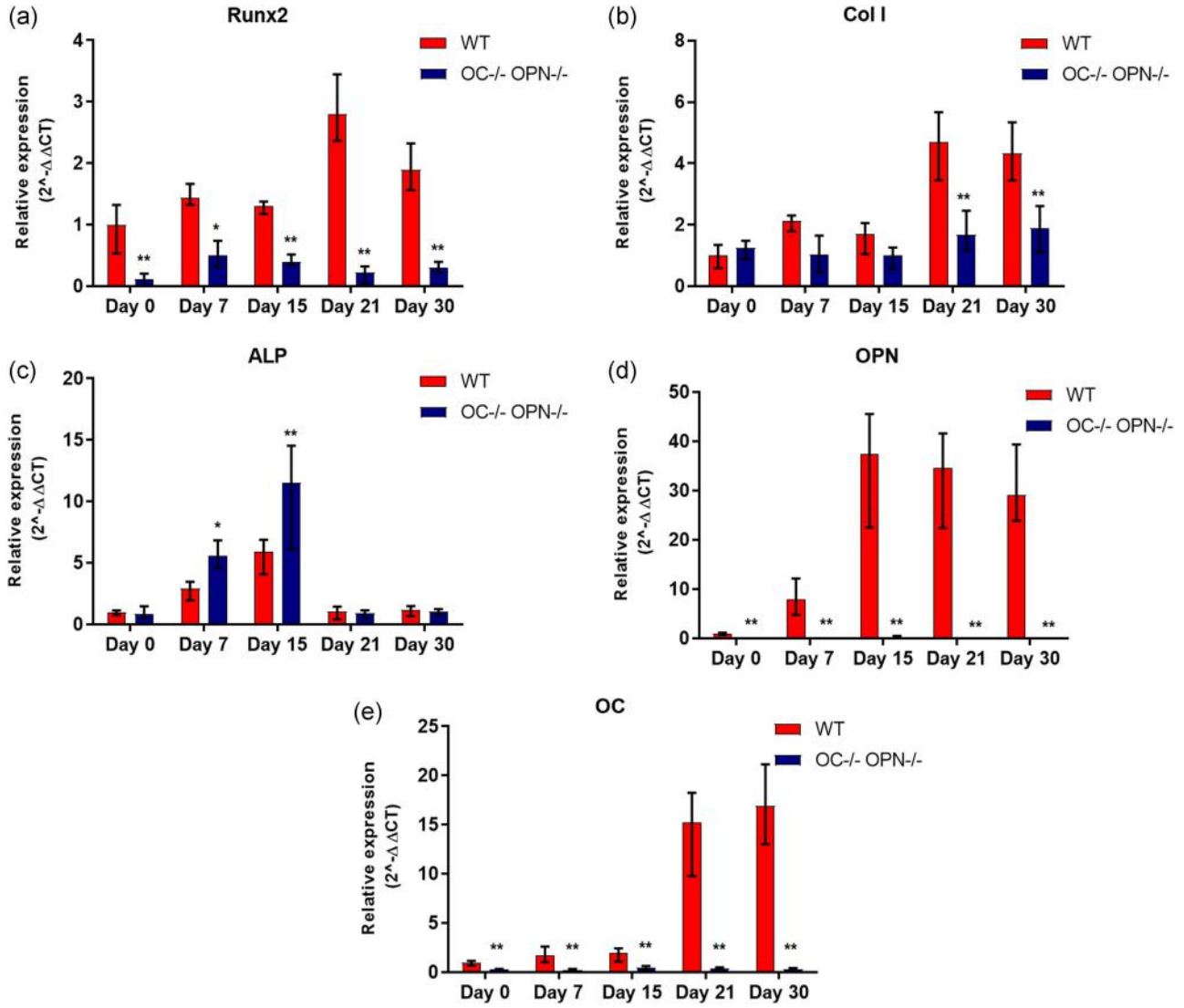

FIGURE 3 Gene expression analysis of $OC^{-/-}$ $OPN^{-/-}$ MSC after osteogenic differentiation. WT and $OC^{-/-}$ $OPN^{-/-}$ MSC cultured in osteogenic differentiation medium for the indicated times were analyzed for (a) Runx2, (b) Col I, (c) ALP, (d) OPN, and (e) OC by qRT- PCR. ALP, alkaline phosphatase; Col I, collagen type I; MSC, mesenchymal stem/stromal cells; OC, osteocalcin; OPN, osteopontin; qRT- PCR, quantitative reverse transcription polymerase chain reaction; Runx2, runt-related transcription factor 2; WT, wild type. $^{**}p < .01$; $^{*}p < .05$

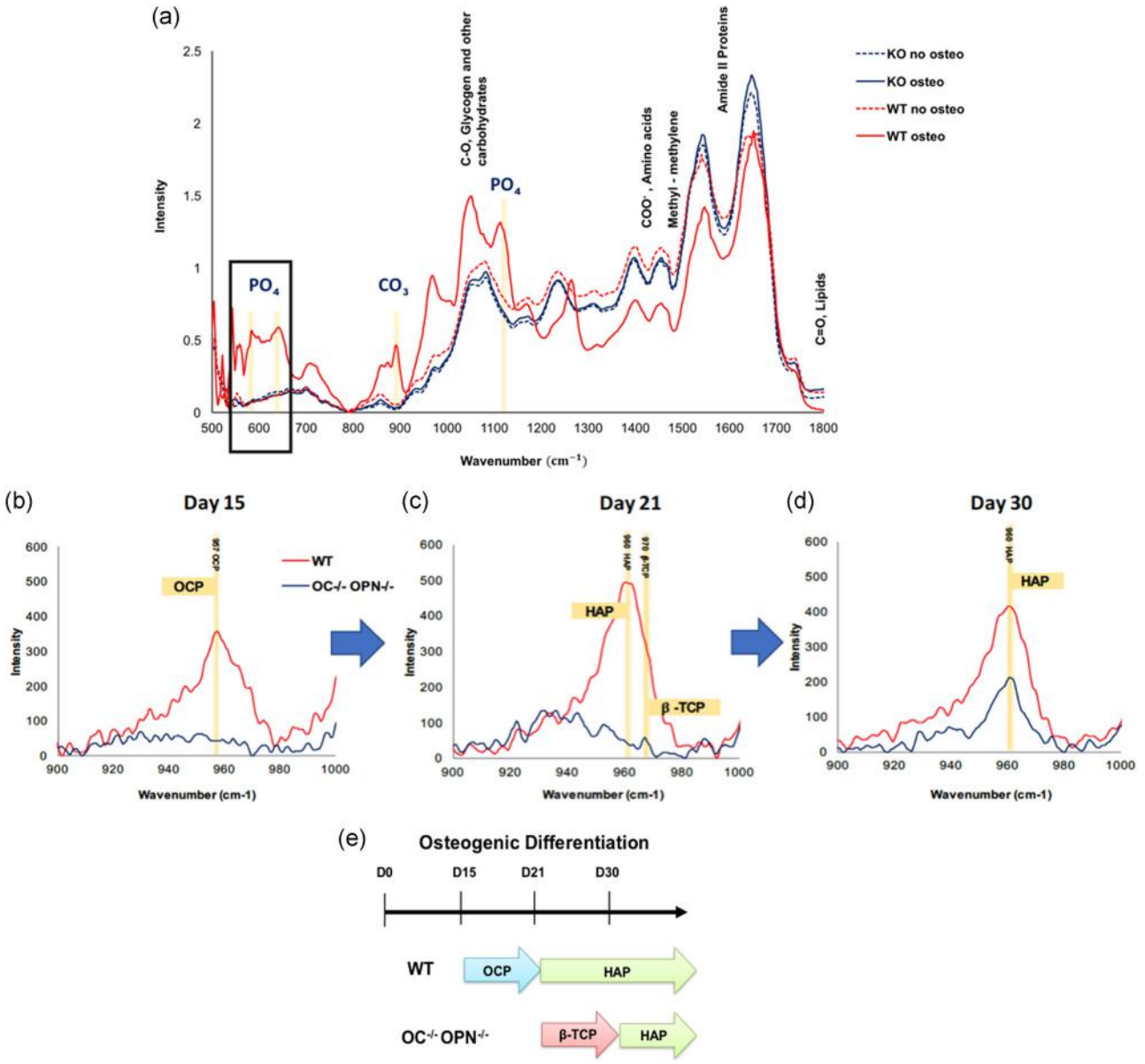

FIGURE 4 Spectroscopy analysis of WT MSC and $OC^{-/-}$ $OPN^{-/-}$ MSC after osteogenic differentiation. (a) FTIR spectra of the WT MSC and $OC^{-/-}$ $OPN^{-/-}$ (KO) MSC without differentiation (no osteo) and after 21 days of differentiation (osteo). The characteristic peaks of amide I (1645 cm^{-1}) and amide II (1550 cm^{-1}), carbohydrates, amino acids, and lipids can be found. (b–d) Raman spectra of mineral species produced by WT and $OC^{-/-}$ $OPN^{-/-}$ MSC after 15 (b), 21 (c), and 30 days (d) of osteogenic differentiation. (e) Temporal progression of the mineral species produced by WT and $OC^{-/-}$ $OPN^{-/-}$ MSC under osteogenic differentiation. MSC, mesenchymal stem/stromal cells; OC, osteocalcin; OPN, osteopontin; WT, wild type

spectra of both cell types after 15, 21, and 30 days of osteogenic differentiation was acquired (Figure 4b–d) and dissected in detail, as depicted in the region from 900 to 1,000 cm^{-1}.

The Raman signal of OCP at 957 cm^{-1} was detected in WT MSC at Day 15 of osteogenic differentiation, however, no detectable peak was observed for $OC^{-/-}$ $OPN^{-/-}$ MSC (Figure 4b). At Day 21 of osteogenic differentiation, the OCP signal could not be detected anymore and, further, WT MSC presented the HAP peak at 960 cm^{-1} (Figure 4c). On the other hand, $OC^{-/-}$ $OPN^{-/-}$ MSC did not present the HAP peak, however, a small signal of β-TCP at 970 cm^{-1}, a HAP precursor, was found after 21 days of differentiation. β-TCP is known to contribute to HAP synthesis, which can be used as an early stage marker of MSC-osteoblast differentiation.

Thus, OCP (957 cm^{-1}) was only observed after 15 days under differentiation conditions for minerals produced by WT MSC and after 21 days of differentiation, HAP minerals were produced by WT MSC (as the HAP peak at 960 cm^{-1} was found). After 7 days under osteogenic differentiation conditions, no detectable peak related to mineral species was found in MSC cultures. Furthermore, after 21 days of differentiation, $OC^{-/-}OPN^{-/-}$ MSC did not produce HAP

minerals, as this peak was not detected (Figure 4c). In contrast, after 21 days under differentiation conditions, a small peak of β-TCP was found indicating that the minerals produced by $OC^{-/-}$ $OPN^{-/-}$ MSC were not mature enough. Using spectroscopic analysis, we confirmed that mineralization was impaired after 21 days under osteogenic differentiation conditions. Raman spectroscopy confirmed that after 21 days under differentiation conditions $OC^{-/-}$ $OPN^{-/-}$ MSC produced less mineral, and that the mineral produced was not sufficiently mature (Figure 4c).

Furthermore, when we extend the duration of differentiation, the Raman spectrum of the mineral produced by $OC^{-/-}$ $OPN^{-/-}$ presented the HAP peak after 30 days of differentiation. Thus, by increasing the duration under which the cells are subjected to differentiation conditions, the mineral content switches to a more mature phase of HAP (Figure 4d). Therefore, OC and OPN are insufficiently expressed under these conditions and the maturation of mineral is delayed (Figure 4e).

The total amount of GAG (Figure 5a), as well as the respective HS, chondroitin sulfate (CS), and hyaluronic acid (HA) GAG amounts (Figure 5b) for WT and $OC^{-/-}$ $OPN^{-/-}$ MSC were obtained after LC-MS/MS analysis. As shown in Figure 5a, $OC^{-/-}OPN^{-/-}$ MSC presented higher GAG content than WT MSC. Regarding HS, CS, and HA total composition, there were evident differences in the GAG compositions of different cell types (Figure 5b). $OC^{-/-}$ $OPN^{-/-}$ MSC were composed mainly by CS (153.3 ± 21.2 ng/ml), followed by lower average amounts of HS (31.1 ± 6.2 ng/ml) and HA (20.9 ± 1.8 ng/ml). In contrast, WT MSC were composed of CS (5.7 ± 0.3 ng/ml), HS (3.8 ± 0.5 ng/ml), and lower amounts of HA (0.2 ± 0.2 ng/ml). Interestingly after 21 days, the total amount of GAG decreased when both types of cells (WT and $OC^{-/-}$ $OPN^{-/-}$ MSC) were maintained under osteogenic differentiation medium. WT MSC, differentiated into an osteogenic lineage, were associated with the production of a very low amount of GAG, compared with $OC^{-/-}$ $OPN^{-/-}$ MSC differentiated under osteogenic conditions.

Both undifferentiated cells (WT and $OC^{-/-}$ $OPN^{-/-}$ MSC) presented significantly different HS, CS, and HA percentage compositions (Figure 5c). However, when both cell types were differentiated into an osteogenic lineage, similar GAG disaccharide percentage composition was observed. In terms of relative percentages of GAG, WT MSC were mainly composed of CS (59 ± 5%), followed closely by HS (39 ± 3%) and HA (2 ± 2%). Moreover, $OC^{-/-}$ $OPN^{-/-}$ MSC presented a higher relative average percentage of CS (75 ± 2%), HA (11 ± 2%), and lower relative average percentages of HS (14 ± 3%) when compared with WT MSC. After 21 days under osteogenic differentiation conditions, both MSC produced mainly CS (WT, 55 ± 3%; $OC^{-/-}$ $OPN^{-/-}$, 58 ± 6%) with lower amounts of HS (WT, 28 ± 3%; $OC^{-/-}$ $OPN^{-/-}$, 25 ± 3%) and HA (WT, 18 ± 3%; $OC^{-/-}$ $OPN^{-/-}$, 18 ± 3%; Figure 5c).

The compositional analysis of the GAG disaccharides of WT and $OC^{-/-}$ $OPN^{-/-}$ MSC is presented in Figure 5d,e. For all the cells, HS was comprised primarily of 0S, followed by NS and N2S (Figure 5d). However, some differences were noticed in the percentage composition of HS disaccharide, present in the different types of cells. $OC^{-/-}$ $OPN^{-/-}$ MSC presented a higher relative percentage of 0S when compared with WT MSC. On the other hand, WT MSC presented higher relative percentage of NS2S and NS than $OC^{-/-}OPN^{-/-}$ MSC. When the cells were differentiated into an osteogenic lineage, the HS relative percentage did not change dramatically. However, WT MSC, differentiated into an osteogenic lineage (WT Osteo), seemed to present higher relative percentage of NS, compared with undifferentiated cells. In terms of CS disaccharides, all the cells were primarily composed of 4S, 6S, and 0S (Figure 5e). The relative percentages of 4S and 0S were quite similar between both the cell types (WT and $OC^{-/-}$ $OPN^{-/-}$ MSC). However, $OC^{-/-}$ $OPN^{-/-}$ MSC presented higher relative percentage of 6S when compared with WT MSC. Notably, when WT MSC were differentiated under osteogenic conditions, the CS relative percentage was similar to undifferentiated cells. However, some differences were observed when $OC^{-/-}$ $OPN^{-/-}$ MSC were differentiated after 21 days under osteogenic conditions (OC/OPN KO Osteo) compared with undifferentiated cells. Of note, the relative percentage of 2S6S and 4S6S increased when $OC^{-/-}$ $OPN^{-/-}$ MSC were differentiated into an osteogenic lineage (Figure 5e). In addition, the relative percentage of 6S and 0S dramatically decreased when the cells were differentiated.

3.5 | Loss of OC and OPN impairs the angiogenic potential of MSC

HUVEC cultured with CM from $OC^{-/-}$ $OPN^{-/-}$ MSC ($OC^{-/-}$ $OPN^{-/-}$ CM) were not able to form a capillary-like network (Figure 6a). Moreover, when cultured with CM from WT MSC (WT CM), HUVEC started to form a network with some branches interconnected, after 8 hr postseeding. HUVEC incubated with EGM-2 was used as positive control, as it contained angiogenic factors that will enable HUVEC to form tubular structures when seeded on Matrigel substrate. Basal DMEM was used as a negative control, as this medium does not contain any important factor for angiogenesis. In particular, WT CM did not increase the number of tubes formed by HUVEC, compared with basal DMEM (medium without angiogenic factors), presenting the same weak tubular-like structures as basal DMEM.

In a different assay, we evaluated if the conditioned medium collected from $OC^{-/-}$ $OPN^{-/-}$ MSC would have any effect on the migratory ability of HUVEC. Therefore, a scratch ("wound") was introduced in a confluent monolayer of HUVEC cultured with CM from WT and $OC^{-/-}$ $OPN^{-/-}$ MSC. EGM-2, added to the cell culture, was used as a positive control. Interestingly, when HUVEC were incubated with CM from WT MSC for 8 hr, the "wound" size decreased due to the migration of HUVEC toward the site (Figure 6c). The same effect was observed for the positive control, EGM-2, due to the angiogenic factors present in this medium. However, when HUVEC were cultured with $OC^{-/-}$ $OPN^{-/-}$ CM, the scratch diameter changed marginally, indicating that HUVEC's migration capability was impaired due to the lack of OC and OPN. Notably, after 12 hr, the wound site was almost closed when HUVEC were cultured with WT CM, presenting a percentage of migration of 77% (Figure 6d). After 12 hr, conditioned

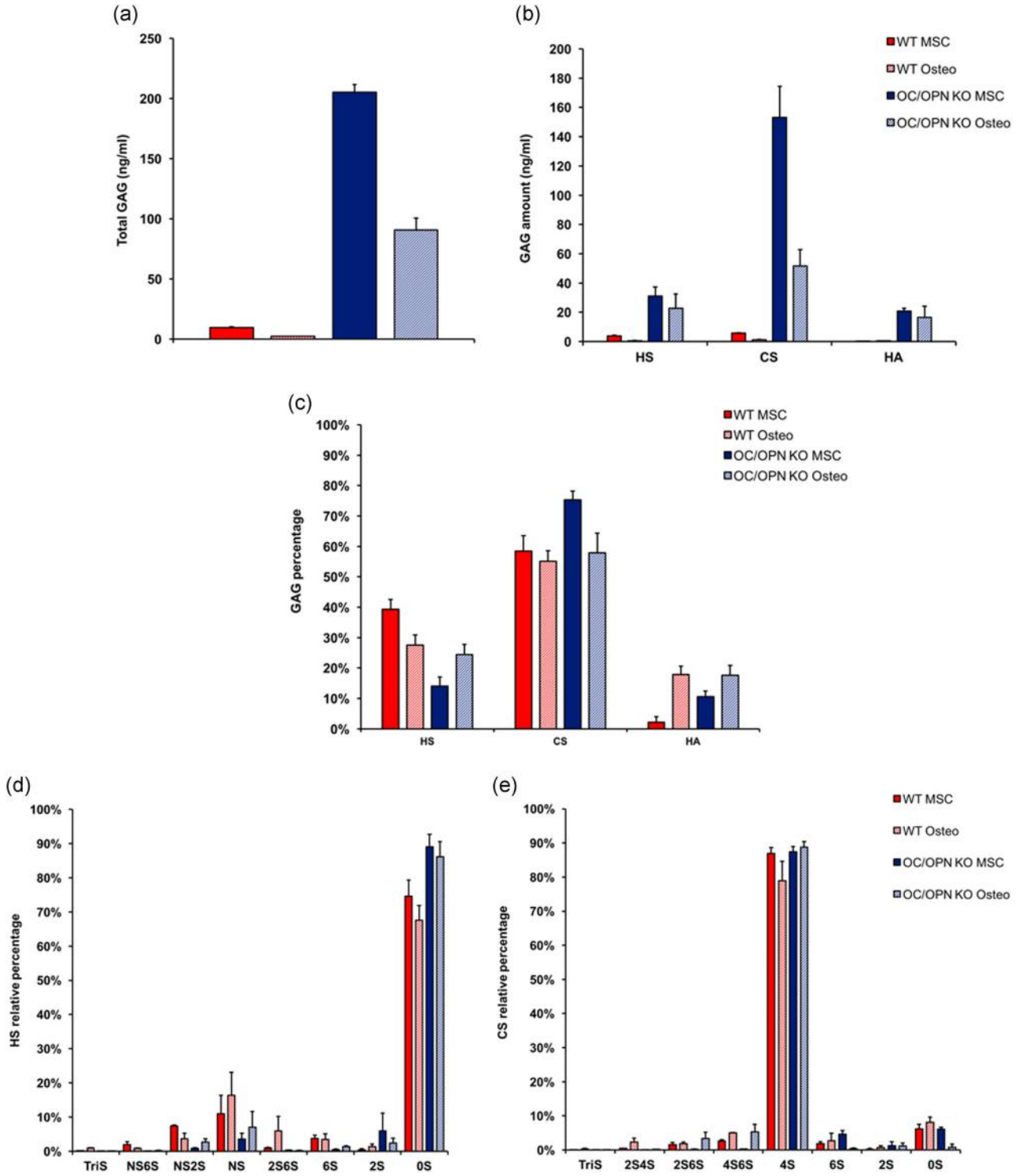

FIGURE 5 GAG composition of WT MSC and $OC^{-/-}$ $OPN^{-/-}$ MSC. (a) Total GAG amount. (b) HS, CS, HA total amounts. (c) Average relative percentage of total GAG composition. (d) HS relative percentage of WT and $OC^{-/-}$ $OPN^{-/-}$ MSC before and after osteogenic differentiation. (e) CS relative percentage of WT and $OC^{-/-}$ $OPN^{-/-}$ MSC before and after osteogenic differentiation. Results are presented as mean ± *SD* of three biological replicates ($n = 3$). CS, chondroitin sulfate; GAG, glycosaminoglycans; HA, hyaluronic acid; HS, heparin sulfate; MSC, mesenchymal stem/stromal cells; OC, osteocalcin; OPN, osteopontin; WT, wild type

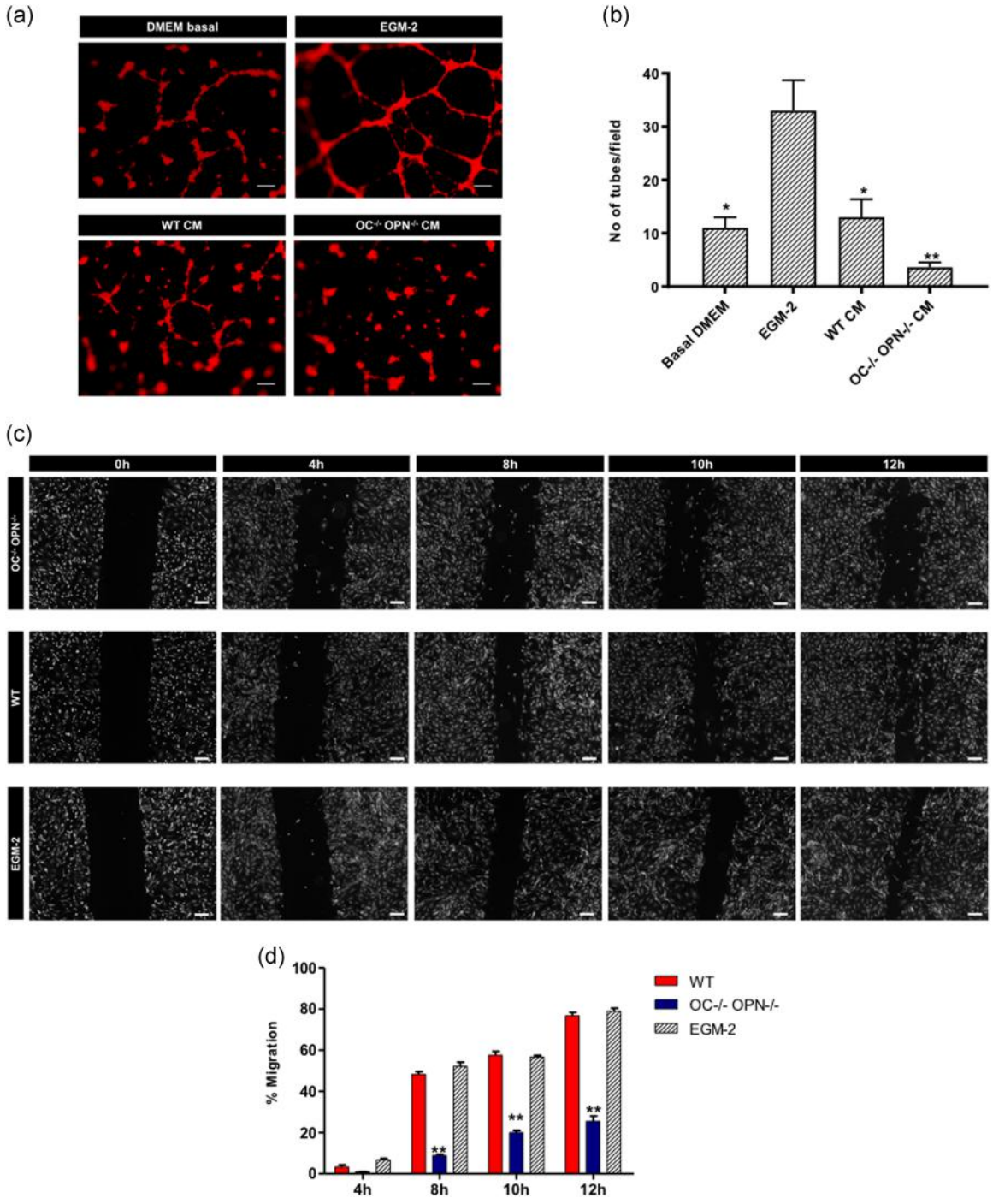

FIGURE 6 OC/OPN deficiency impairs angiogenic properties of MSC. (a) Tube formation assay evaluating the HUVEC's response to conditioned medium (CM) from $OC^{-/-}OPN^{-/-}$ MSC after 8 hr postseeding. (b) Number of tubes formed by HUVEC in the tube formation assay. (c) Migration assay evaluating the HUVEC's migratory response to CM from $OC^{-/-}OPN^{-/-}$ MSC after 4, 8, 10, and 12 hr. (d) Quantification of the HUVEC's percentage of migration after different timepoints when exposed to different conditioned medium from WT and $OC^{-/-}$ $OPN^{-/-}$ MSC. DMEM + 10% FBS and EGM-2 were used as a positive control and DMEM basal as a negative control. Scale bar = 100 μm. Values are mean ± *SD*. CM, conditioned medium; DMEM, Dulbecco's modified Eagle's medium; EGM-2, endothelial growth medium-2; FBS, fetal bovine serum; HUVEC, human umbilical vein endothelial cells; MSC, mesenchymal stem/stromal cells; OC, osteocalcin; OPN, osteopontin; WT, wild type. $^{**}p < .01$; $^{*}p < .05$ compared with EGM-2 (positive control)

medium from $OC^{-/-}$ $OPN^{-/-}$ MSC allowed only a 26% percentage of migration (Figure 6c,d).

Furthermore, the angiogenic potential of WT MSC and $OC^{-/-}$ $OPN^{-/-}$ MSC was also evaluated by performing a functional tube formation assay with a coculture of MSC and HUVEC (Figure 7a). As expected, HUVEC alone were able to form a capillary-like structure after 2 hr, as HUVEC were cultured with EGM-2 medium, containing angiogenic factors. Later, 4 hr after seeding, the network structure

became more robust with interconnected branches. After 24 hr, the tube's length increased while maintaining the capillary-like structure (Figure 7b). Coculture of WT MSC and HUVEC demonstrated the same pattern as HUVEC alone, allowing HUVEC to form a well-defined capillary-like structure (Figure 7b). Notably, when $OC^{-/-}$ $OPN^{-/-}$ MSC were cocultured with HUVEC, HUVEC started to form tubes after 2 hr, however, after 8 hr, the tubular structures were maintained and were consequently disrupted, as shown in Figure 7b. After 24 hr, the tubes were completely destroyed. Therefore, we confirmed that the absence of OC and OPN would impair the angiogenic capacity of MSC, as the coculture of $OC^{-/-}$ $OPN^{-/-}$ MSC with HUVEC was not able to maintain and support the tubular-like structure formed by HUVEC. In contrast, WT MSC cocultured with HUVEC were able to sustain their tubular morphology.

To identify the protein that was responsible for the impairment of the angiogenic capacity of HUVEC, we cocultured $OC^{-/-}$ $OPN^{-/-}$ MSC with HUVEC and supplemented the medium with OC and/or OPN. When OC and OPN (1 μg/ml each protein) were added to the system, as well as just OPN, HUVEC that were cocultured with $OC^{-/-}$ $OPN^{-/-}$ MSC were able to form tubular-like structures. However, when only OC was supplemented to the cell culture, HUVEC did not form the same capillary-like structure. (Figure 7c). Figure 7d showed that the number of tubes formed by HUVEC cocultured with $OC^{-/-}$ $OPN^{-/-}$ MSC exogenously supplemented with OPN and OPN/OC increased, compared with HUVEC cocultured with $OC^{-/-}$ $OPN^{-/-}$ MSC without OC/OPN

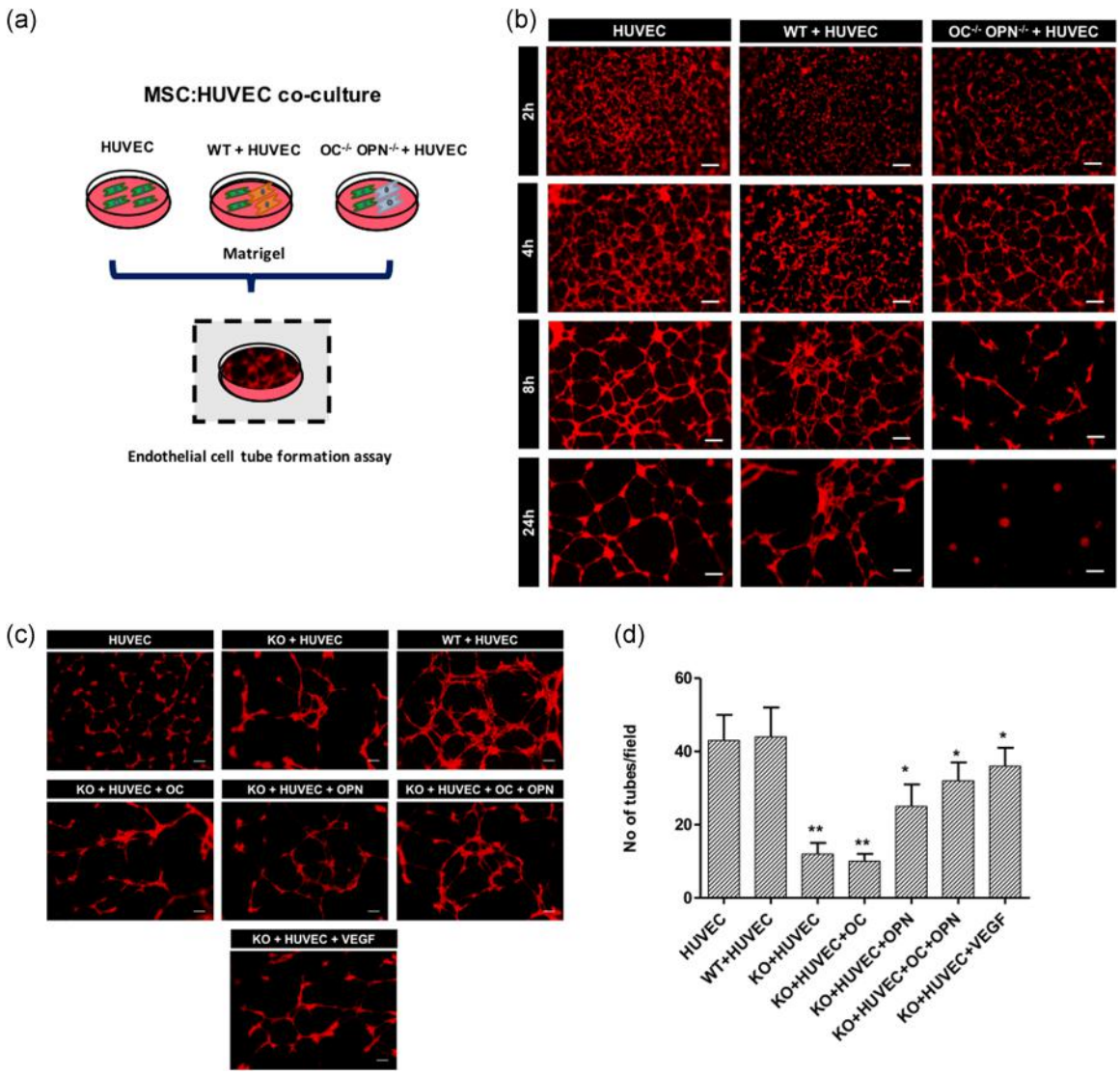

FIGURE 7 Angiogenic properties of $OC^{-/-}$ $OPN^{-/-}$ MSC. (a) Schematic figure of endothelial cell tube formation assay: WT MSC and $OC^{-/-}$ $OPN^{-/-}$ cocultured with HUVEC. (b) HUVEC tubular structure formed in the absence and presence of $OC^{-/-}$ $OPN^{-/-}$ MSC or WT MSC after 2, 4, 8, and 24 hr. (c) Coculture of $OC^{-/-}$ $OPN^{-/-}$ MSC with HUVEC supplemented with OC and/or OPN and VEGF. Scale bar = 100 μm. (d) Quantification of number of tubes formed by HUVEC cocultured with $OC^{-/-}$ $OPN^{-/-}$ (KO) MSC supplemented with OC and/or OPN and VEGF. Values are expressed as mean ± *SD*. HUVEC, human umbilical vein endothelial cells; KO, knockout; MSC, mesenchymal stem/stromal cells; OC, osteocalcin; OPN, osteopontin; VEGF, vascular endothelial growth factor; WT, wild type. $^{**}p < .01$; $^{*}p < .05$, compared with HUVEC

supplementation. HUVEC cocultured with WT MSC demonstrated a more robust tubular morphology with more interconnected tubes, leading us to conclude that exogenous supplementation of OPN as a compensatory strategy did not present the same enhanced results as WT MSC. HUVEC cocultured with WT MSC showed a significant tube formation on Matrigel, whereas only few tubes were formed by HUVEC cocultured with $OC^{-/-}$ $OPN^{-/-}$ MSC (Figure 7c,d).

3.6 | Rescue of the proliferative and osteogenic potential of MSC by OC/OPN extracellular supplementation

After OC treatment, no significant increase in proliferation was observed. However, after OPN, as well as OC/OPN treatment, MSC recovered their proliferative potential, increasing cell number after 4 days of culture (Figure 8a). Indeed, $OC^{-/-}$ $OPN^{-/-}$ MSC supplemented with OC and OPN or only with OPN presented similar growth rate as WT MSC, reaching the same cell number after 15 days of proliferation (Figure 8a). This result suggested that OPN might act on proliferative capacity of $OC^{-/-}$ $OPN^{-/-}$ MSC, however, OC failed to induce proliferation under the conditions tested. Exogenous supplementation of OC/OPN in the osteogenic differentiation medium enabled the MSC to regain their capacity for osteogenic differentiation, shown by the significant increase in calcium deposition, quantified and visualized using Xylenol Orange stain (Figure 8b,c). Although mineralization was enhanced, the results obtained by $OC^{-/-}$ $OPN^{-/-}$ MSC supplemented with OC/OPN did not completely achieve the results obtained with WT MSC. Interestingly, after 21 days under osteogenic differentiation conditions, Raman spectroscopy demonstrated that the mineral formed by $OC^{-/-}$ $OPN^{-/-}$ MSC supplemented exogenously with OC/OPN was composed of HAP, as observed for mineral species produced by WT MSC. In contrast, the mineral generated by $OC^{-/-}$ $OPN^{-/-}$ MSC (without exogenous supplementation of 1 μg/ml of OC/OPN) did not present the HAP peak, suggesting a more immature mineral production (Figure 8d).

4 | DISCUSSION

OC and OPN are major noncollagenous proteins known to play an important role in bone mineralization. These proteins are involved in

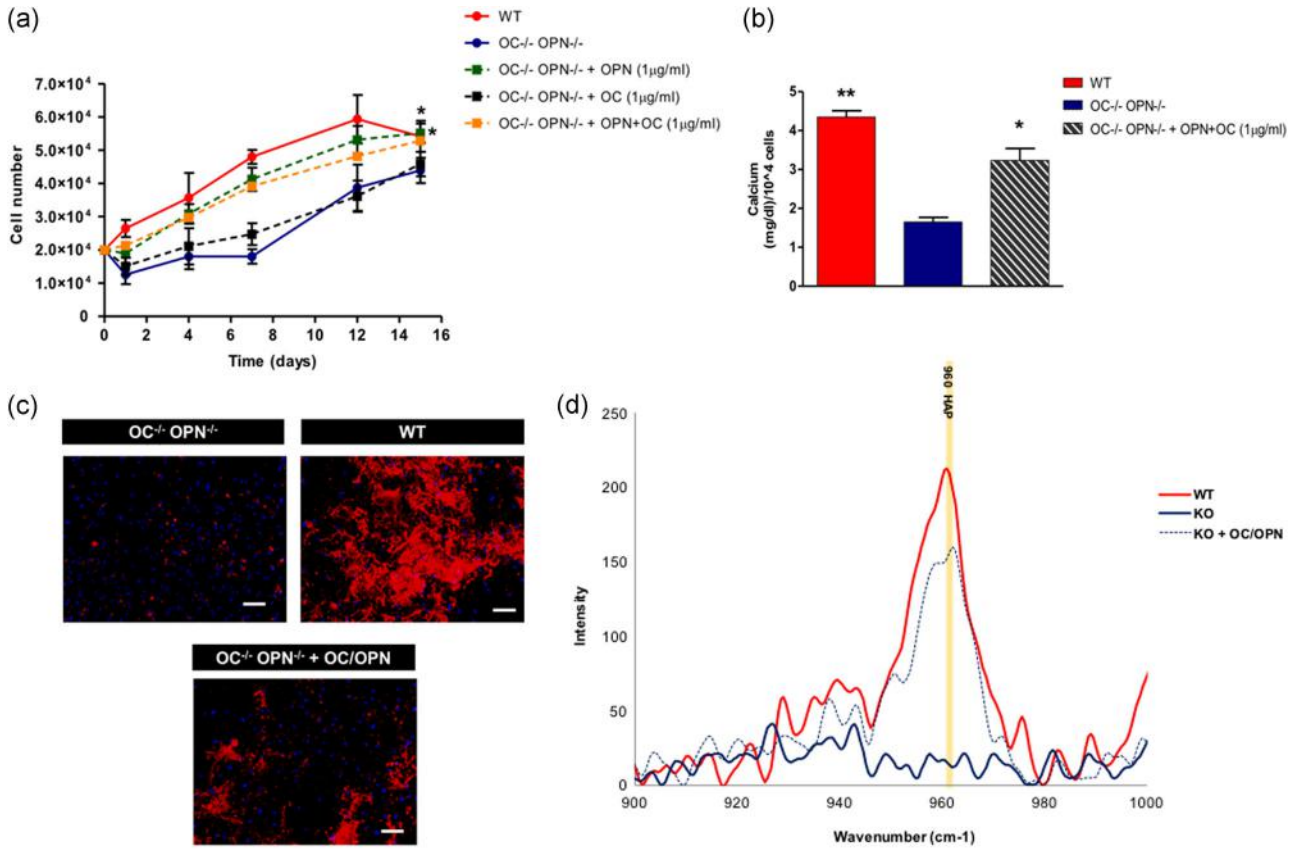

FIGURE 8 Effects of OC/OPN supplemented extracellularly on $OC^{-/-}OPN^{-/-}$ MSC proliferation and osteogenic potential. (a) Proliferation of $OC^{-/-}OPN^{-/-}$ MSC exogenously supplemented with OC and/or OPN (1 μg/ml). (b) Calcium quantification of $OC^{-/-}OPN^{-/-}$ MSC differentiated during 21 days with osteogenic medium supplemented with OC/OPN (1 μg/ml). (c) Calcium deposits from $OC^{-/-}OPN^{-/-}$ MSC supplemented with OC/OPN were visualized using Xylenol Orange (blue, DAPI). (d) Comparison of Raman spectrum of WT, $OC^{-/-}$ $OPN^{-/-}$ and $OC^{-/-}$ $OPN^{-/-}$ MSC extracellularly supplemented with OC/OPN. Scale bar = 100 μm. Values are means ± *SD*. DAPI, 4′,6-diamidino-2-phenylindole; MSC, mesenchymal stem/stromal cells; OC, osteocalcin; OPN, osteopontin; WT, wild type. $^{**}p < .01$.$^{*}p < .05$, compared with $OC^{-/-}$ $OPN^{-/-}$

bone matrix organization and deposition. Several studies from our group have reported that OC and OPN influence bone morphology and mechanical properties (Bailey et al., 2017; Morgan, Poundarik, & Vashishth, 2015; Nikel, Poundarik, Bailey, & Vashishth, 2018; Poundarik, Boskey, Gundberg, & Vashishth, 2018; Poundarik et al., 2012). Bone morphology of either $OC^{-/-}$ or $OPN^{-/-}$ single knockout mice is not different from each other or from WT mice but bones from mice lacking both OC and OPN ($OC^{-/-}$ $OPN^{-/-}$) are shorter, with thicker cortices and larger cortical areas compared with WT and single knockout $OC^{-/-}$ and $OPN^{-/-}$ groups, suggesting a synergistic role of OC/OPN in determining bone morphology (Bailey et al., 2017). We also observed that the removal of both proteins induced morphological adaptations at the structural level, maintaining bone strength but causing loss of toughness due to loss of energy dissipating mechanisms at nanoscale (Bailey et al., 2017; Poundarik et al., 2012). Here, we investigate the synergistic effect of these two proteins at the cellular level by evaluating MSC derived from $OC^{-/-}$ $OPN^{-/-}$ mice. Single knockout mice models (e.g., $OPN^{-/-}$ or $OC^{-/-}$) alone fail to elucidate the specific roles of noncollagenous proteins in the different cellular processes, as the loss of one protein may be compensated by the other. Therefore, we isolated MSC from the bone marrow of $OC^{-/-}$ $OPN^{-/-}$ mice and characterized these cells, investigating the roles of OC and OPN on the proliferation, differentiation, and pro-angiogenic potential of MSC in vitro.

$OC^{-/-}$ $OPN^{-/-}$ MSC demonstrated the same immunophenotype as WT MSC, expressing CD29, CD105, Sca-1, and lower levels of CD45. However, we observed that the proliferative potential of $OC^{-/-}$ $OPN^{-/-}$ MSC was impaired by the lack of OC and OPN, compared with WT MSC. A kinetic study demonstrated a slower growth rate for $OC^{-/-}$ $OPN^{-/-}$ MSC compared with WT MSC, reaching lower cell numbers. Several reports have shown that OPN exerts an important effect on different types of cells, increasing the proliferation of tumor cells (Saleh, Thompson, McConkey, Murray, & Moorehead, 2016), neural stem cells (Rabenstein et al., 2015), vascular smooth muscle cells (Lee, Baek, Jang, & Kim, 2016), hepatic progenitor cells (Liu et al., 2015), and MSC (Carvalho, Cabral, da Silva, & Vashishth, 2019). Therefore, we hypothesized that the lack of secreted OPN was, indeed, responsible for the impaired proliferation observed by $OC^{-/-}$ $OPN^{-/-}$ MSC. Supplementation of the culture medium with only OPN or OC/OPN allowed $OC^{-/-}$ $OPN^{-/-}$ MSC to rescue their proliferative potential. More important, we confirmed that lack of OPN was responsible for the impairment of proliferation capacity observed by $OC^{-/-}$ $OPN^{-/-}$ MSC since when only OC was added to the culture medium $OC^{-/-}$ $OPN^{-/-}$ MSC did not enhance proliferation.

Given a slower growth rate of $OC^{-/-}$ $OPN^{-/-}$ MSC but similar immunophenotype compared with WT MSC, further characterization of these cells with respect to ECM was done. GAG are the major constituents of proteoglycans and can be found in multiple tissues including, but not limited to, cartilage and bone. In addition, the sulfation patterns in GAG chains facilitate interactions with growth factors, cell surface receptors, enzymes, cytokines, and chemokines associated with several biological processes, such as development, cell growth, and differentiation (Gasimli et al., 2014; Papy-Garcia & Albanese, 2017; Wang et al., 2017). Here, we showed that knocking out OC and OPN genes enhanced production of GAG by differentiated MSC. We used a previously developed method of liquid chromatography-tandem mass spectrometry (LC-MS/MS) with MRM (Silva et al., 2019; Sun et al., 2015) to characterize $OC^{-/-}$ $OPN^{-/-}$ MSC and WT MSC for GAG content, composition, and sulfation pattern. $OC^{-/-}$ $OPN^{-/-}$ MSC were mainly composed of CS and produced higher amounts and relative percentages of this GAG than WT MSC. Interestingly, the amount of GAG produced by $OC^{-/-}$ $OPN^{-/-}$ MSC increased dramatically compared with WT MSC. As OC and OPN are the most abundant noncollagenous bone proteins present in bone matrix, lack of these proteins could induce the production of other important noncollagenous bone matrix proteins to compensate the absence of OC/OPN. Therefore, we hypothesize that bone ECM increases its GAG content as a compensatory mechanism, synthesizing a matrix richer in GAG. Each cell type secretes unique and specific ECM to fulfill the biological requirements of its native tissue. However, we observed that despite the differences in content, the relative percentage (CS, HS, HA) produced by $OC^{-/-}$ $OPN^{-/-}$ MSC was quite similar to WT. Our results indicate that, in terms of CS disaccharides, all cell types, undifferentiated and differentiated, were mainly composed of 4S. Consistent with our results, others have shown that CS4S disaccharide represent the major GAG present in bone tissue (Engfeldt & Hjerpe, 1976; Mania et al., 2009; Waddington, Embery, & Last, 1989). We believe that the decrease of GAG content seen in WT MSC, associated with osteogenic differentiation, is due to the deposition of a more mature mineralized matrix. In fact, Engfeldt and Hjerpe demonstrated that the total amount of GAG in bone tissue, mainly CS, seems to decrease while the degree of mineralization increases (Engfeldt & Hjerpe, 1976). Consequently, increased GAG observed with $OC^{-/-}$ $OPN^{-/-}$ MSC represents delayed bone mineralization, associated with a more primitive skeletal connective tissue (Engfeldt & Hjerpe, 1976). These results provide an interesting insight into skeletal evolution as both OC and OPN—named based on their association and discovery in the bone—are thought to be associated with the evolution of bone formed by peri- and endo-chondral ossification (Hall, 2005).

Consistent with the above hypothesis, we observed that, although adipogenic and chondrogenic differentiation did not change, osteogenic differentiation of $OC^{-/-}$ $OPN^{-/-}$ MSC was delayed when compared with WT. Lower amount of calcium levels, as well as micrographs of the mineral produced by $OC^{-/-}$ $OPN^{-/-}$ MSC, demonstrated an impairment of mineral production by these double knockout cells. Moreover, the gene expression levels of osteogenic markers demonstrated that $OC^{-/-}$ $OPN^{-/-}$ MSC downregulated most of the osteogenic genes, such as *Runx2*, *Col I*, *OC*, and *OPN*.

To better understand the quality of the mineral produced by these cells, we analyzed the mineral using both FTIR and Raman spectroscopy. Results showed that after 21 days under osteogenic differentiation conditions, FTIR spectra of minerals produced by $OC^{-/-}$ $OPN^{-/-}$ MSC did not show the absorption peaks associated with major bone-related molecular species, such as phosphate and

carbonate, seen with WT MSC. FTIR spectra of WT and $OC^{-/-}$ $OPN^{-/-}$ MSC demonstrated absorption peaks associated with cellular components, such as amide groups, carbohydrates, and amino acids before and after osteogenic differentiation. Using Raman spectroscopy, we were able to show that after 15 days under osteogenic differentiation conditions, WT MSC were able to produce OCP (957 cm^{-1}), a HAP precursor, whereas the minerals produced by $OC^{-/-}$ $OPN^{-/-}$ MSC did not present the OCP peak. Previous studies have demonstrated that OCP is the precursor of mineralized matrix at the early stage mineralization and it also participates in HAP synthesis during bone formation (Anada et al., 2008). Indeed, after 21 days of osteogenic differentiation, HAP was detected in the minerals produced by WT cells, indicating a late and more advanced stage of differentiation. However, $OC^{-/-}$ $OPN^{-/-}$ MSC did not present HAP peak (960 cm^{-1}), instead a β-TCP peak was detected (970 cm^{-1}), also a HAP precursor. Notably, the HAP peak was only detected in the minerals produced by $OC^{-/-}$ $OPN^{-/-}$ MSC after 30 days under osteogenic differentiation conditions.

We observed that the maturation of mineral species produced by $OC^{-/-}$ $OPN^{-/-}$ MSC was delayed compared with the control group. These results confirm that, at a cellular level, OC and OPN are important regulators of bone mineralization during osteogenic differentiation of MSC. Moreover, these results demonstrate that Raman spectroscopy is a powerful tool to measure the maturation level of MSC-osteoblast differentiation by detecting the intensity changes of mineral components in MSC. In fact, during the crystal growth phase of the biomineralization process, OC has been reported to accelerate the nucleation of HAP and inhibit HAP precipitation (Ducy et al., 1996). Previous studies have already reported that both OC and OPN have specific roles in the biomolecular regulation of mineral in bone and together they are major determinants of bone mineral quality (Poundarik, Boskey, Gundberg, & Vashishth, 2018). Poundarik and colleagues have shown that OC and OPN regulate bone mineral crystal size and organization in a codependent manner (Poundarik, Boskey, Gundberg, & Vashishth, 2018). Our data demonstrates that the inhibition of osteogenesis is associated with the downregulation of osteogenic gene markers involved in osteogenesis, such as *Runx2*, *Col I*, *OC*, and *OPN*.

Our studies also demonstrated that the osteogenic potential of $OC^{-/-}$ $OPN^{-/-}$ MSC was recovered when OC/OPN were exogenously supplemented. After 21 days of osteogenic differentiation, when OC/OPN were exogenously added to the culture medium, minerals produced by $OC^{-/-}$ $OPN^{-/-}$ cells were mainly composed of HAP (960 cm^{-1}), similar to the minerals produced by WT MSC. However, despite the addition of both OC/OPN proteins to the medium, $OC^{-/-}$ $OPN^{-/-}$ MSC continued to produce lower amount of calcium level compared with WT MSC. Therefore, further studies should be performed to unveil the most beneficial OC/OPN dose to recover the osteogenic potential of $OC^{-/-}$ $OPN^{-/-}$ MSC. These data suggest that OC and OPN exert its regulatory role in MSC differentiation in an intra- and extracellular manner and they can rescue the bone mineral quality. Consequently, the bone tissue engineering applications can benefit from addition of these proteins (Carvalho, Poundarik, Cabral, da Silva, & Vashishth, 2018), as these proteins are lost and/or modified with aging (Nikel, Poundarik, Bailey, & Vashishth, 2018; Sroga & Vashishth, 2018).

As some noncollagenous proteins, such as OPN, have been reported to participate in the recruitment and migration of cells (Rabenstein et al., 2015; Tuck, Hota, Wilson, & Chambers, 2003), we hypothesized that the lack of OPN and OC in MSC will impair the migration of MSC. Introduction of a wound scratch assay in our model demonstrated that conditioned medium from $OC^{-/-}$ $OPN^{-/-}$ MSC did not promote the migration of HUVEC after 12 hr, unlike the conditioned medium from WT MSC. We, therefore, concluded that lack of OC and OPN negatively influenced the migration of HUVEC. Using the same approach in a tube formation assay, we observed that angiogenic capacities of HUVEC are diminished when conditioned medium from $OC^{-/-}$ $OPN^{-/-}$ was used. However, the mechanism of action related with the reduction of angiogenic potential should be further studied. We hypothesize that the lack of OC and OPN compromises the amount and composition of other cytokines and soluble factors in the conditioned medium of $OC^{-/-}$ $OPN^{-/-}$ MSC. For example, OPN is known to induce VEGF expression (Ramchandani & Weber, 2015). Thus, lack of OPN in the culture medium could downregulate the amount of VEGF or other angiogenic factors, and consequently, diminishes the angiogenic potential.

We also observed that when HUVEC were cocultured with WT MSC or $OC^{-/-}$ $OPN^{-/-}$ MSC, HUVEC started to form tubular-like structures after 4 hr. However, after 8 hr, HUVEC cocultured with $OC^{-/-}$ $OPN^{-/-}$ MSC were not able to sustain and support their interconnected network, and after 24 hr the tubes were completely destroyed and only sparse agglomerates of HUVEC were observed. In fact, OPN is a potent angiogenic factor, which promotes proliferation, migration, and capillary-like formation of endothelial cells (Dai et al., 2009), while OC has also been reported to stimulate angiogenesis in vivo (Cantatore, Crivellato, Nico, & Ribatti, 2005). Therefore, we believe that the lack of OPN and OC is responsible for the loss of HUVEC tubular structure. To confirm our hypothesis, we supplemented the coculture of HUVEC and $OC^{-/-}$ $OPN^{-/-}$ MSC with OC and/or OPN. When HUVEC were cocultured with WT MSC a more robust and interconnected capillary-like structure was created. However, when HUVEC were cocultured with $OC^{-/-}$ $OPN^{-/-}$ MSC and supplemented extracellularly with OPN, their tubular structure was able to be sustained after 8 hr. The number of tubes formed after 8 hr, when OPN and OPN/OC were added extracellularly, were significantly higher compared with the $OC^{-/-}$ $OPN^{-/-}$ control (HUVEC + $OC^{-/-}OPN^{-/-}$ MSC) and yielded results similar to those obtained when HUVEC and $OC^{-/-}$ $OPN^{-/-}$ MSC cocultures were supplemented with VEGF. Therefore, we believe that OPN is important for the angiogenic capacity of MSC and that it acts directly or indirectly through the stimulation of other angiogenic factors.

Taken together, these results confirm that, at a cellular level, OC and OPN are important regulators of mineralization and angiogenesis, two important mechanisms for bone repair, and these findings provide new insights into forming high quality bone, relevant for

treatment of fracture healing in older and osteoporotic bone lacking or containing limited OC and OPN. OC/OPN deficiency impairs the proliferation, osteogenic differentiation, mineralization, and angiogenic potential of MSC. Furthermore, we show that most commonly used techniques to confirm osteogenic differentiation rely on using osteogenic gene expression and histological staining techniques. However, these do not capture the quality of bone-like calcium phosphate mineral produced by differentiated cells. Therefore, techniques such as FTIR and Raman spectroscopy should be used to verify the presence and quality of the mineral formed. In this study, we also developed and applied a protocol to evaluate the maturation level of the minerals and matrix produced by MSC at different timepoints of osteogenic differentiation, providing new insights in the quality and composition of the mineral produced in vitro. Overall, these results highlight the key contributions of OC and OPN at enhancing osteogenesis and angiogenesis over primitive connective tissue and support a potential therapeutic approach based on their exogenous supplementation.

ACKNOWLEDGMENTS

This study was supported by funds from NIH grant AR49635 (D.V.), the Center of Biotechnology and Interdisciplinary Studies, Rensselaer Polytechnic Institute, and the FCT (individual fellowship SFRH/BD/52478/2014 awarded to Marta S. Carvalho and individual fellowship SFRH/BD/105771/2014 awarded to João C. Silva). Funding received by iBB-Institute for Bioengineering and Biosciences from FCT (UID/BIO/04565/2019), from Programa Operacional Regional de Lisboa 2020 (Project N. 007317) is also acknowledged. The authors thank Dr. Brigitte Arduini (Rensselaer Polytechnic Institute) for assistance with stem cell isolation and Dr. Sergey Pryshchep (Rensselaer Polytechnic Institute) for assistance with flow cytometry.

DISCLOSURES

Patent application (US serial No. 15/570,942) was filed under 35 U.S.C. § 371 of International application number PCT/US2016/030410 by Rensselaer Polytechnic Institute with M.S.C. and D.V. as inventors. D.V. is the cofounder of Orthograft LLC that is exploring applications of PCT/US2016/030410 for bone regeneration. No other authors have a relevant financial conflict of interest.

AUTHOR CONTRIBUTIONS

M. S. C., C. L. S., D. V. contributed to the conception and design of the experiments. M. S. C., J. C. S., C. M. H. contributed to the execution of the experiments. M. S. C. and D. V. contributed to the analysis of the experiments and drafted the manuscript. All authors participated in reviewing and editing of the final manuscript.

DATA AVAILABILITY STATEMENT

The datasets used and/or analyzed during the current study are available from the corresponding author with reasonable request.

ORCID

Marta S. Carvalho http://orcid.org/0000-0003-1026-1995
João C. Silva http://orcid.org/0000-0003-4773-6771
Joaquim M. S. Cabral http://orcid.org/0000-0002-2405-5845
Robert J. Linhardt http://orcid.org/0000-0003-2219-5833
Cláudia L. da Silva http://orcid.org/0000-0002-1091-7651

REFERENCES

Anada, T., Kumagai, T., Honda, Y., Masuda, T., Kamijo, R., Kamakura, S., … Suzuki, O. (2008). Dose-dependent osteogenic effect of octacalcium phosphate on mouse bone marrow stromal cells. *Tissue Engineering. Part A*, *14*, 965–978. https://doi.org/10.1089/tea.2007.0339

Bailey, S., Karsenty, G., Gundberg, C., & Vashishth, D. (2017). Osteocalcin and osteopontin influence bone morphology and mechanical properties. *Annals of the New York Academy of Sciences*, *1409*, 74–84. https://doi.org/10.1111/nyas.13470

Boskey, A., Maresca, M., & Appel, J. (1989). The effects of noncollagenous matrix proteins on hydroxyapatite formation and proliferation in a collagen gel system. *Connective Tissue Research*, *21*, 171–176. https://doi.org/10.3109/03008208909050007

Boskey, A. L. (1992). Mineral–matrix interactions in bone and cartilage. *Clinical Orthopaedics and Related Research*, *281*, 244–274.

Boskey, A. L., & Coleman, R. (2010). Aging and bone. *Journal of Dental Research*, *89*, 1333–1348. https://doi.org/10.1177/0022034510377791

Cantatore, F. P., Crivellato, E., Nico, B., & Ribatti, D. (2005). Osteocalcin is angiogenic in vivo. *Cell Biology International*, *29*, 583–585. https://doi.org/10.1016/j.cellbi.2005.03.011

Carvalho, M. S., Cabral, J. M. S., da Silva, C. L., & Vashishth, D. (2019). Synergistic effect of extracellularly supplemented osteopontin and osteocalcin on stem cell proliferation, osteogenic differentiation and angiogenic properties. *Journal of Cellular Biochemistry*, *120*, 6555–6569. https://doi.org/10.1002/jcb.27948

Carvalho, M. S., Poundarik, A. A., Cabral, J. M. S., da Silva, C. L., & Vashishth, D. (2018). Biomimetic matrices for rapidly forming mineralized bone tissue based on stem cell-mediated osteogenesis. *Scientific Reports*, *8*, 14388. https://doi.org/10.1038/s41598-018-32794-4

Chen, Q., Shou, P., Zhang, L., Xu, C., Zheng, C., Han, Y., … Shi, Y. (2014). An osteopontin–Integrin interaction plays a critical role in directing adipogenesis and osteogenesis by mesenchymal stem cells. *Stem Cells*, *32*, 327–337.

Dai, J., Peng, L., Fan, K., Wang, H., Wei, R., Ji, G., … Guo, Y. (2009). Osteopontin induces angiogenesis through activation of PI3K/AKT and ERK1/2 in endothelial cells. *Oncogene*, *28*, 3412–3422. https://doi.org/10.1038/onc.2009.189

DeFranco, D. J., Glowacki, J., Cox, K. A., & Lian, J. B. (1991). Normal bone particles are preferentially resorbed in the presence of osteocalcin-deficient bone particles in vivo. *Calcified Tissue International*, *49*, 43–50. https://doi.org/10.1007/BF02555901

Denhardt, D. T., & Guo, X. (1993). Osteopontin: A protein with diverse functions. *The FASEB Journal*, *7*, 1475–1482.

Ducy, P., Desbois, C., Boyce, B., Pinero, G., Story, B., Dunstan, C., … Karsenty, G. (1996). Increased bone formation in osteocalcin-deficient mice. *Nature*, *382*, 448–452. https://doi.org/10.1038/382448a0

Egusa, H., Kayashima, H., Miura, J., Uraguchi, S., Wang, F., Okawa, H., … Yatani, H. (2014). Comparative analysis of mouse-induced pluripotent stem cells and MSC during osteogenic differentiation in vitro. *Stem Cells and Development*, *23*, 2156–2169. https://doi.org/10.1089/scd.2013.0344

Engfeldt, B., & Hjerpe, A. (1976). Glycosaminoglycans of human bone tissue at different stages of mineralization. *Acta Pathologica Microbiologica Scandinavica Section A Pathology*, *84*, 95–106.

Gasimli, L., Hickey, A. M., Yang, B., Li, G., Dela Rosa, M., Nairn, A. V., … Linhardt, R. J. (2014). Changes in glycosaminoglycan structure on differentiation of human embryonic stem cells towards mesoderm and endoderm lineages. *Biochimica et Biophysica Acta*, *1840*, 1993–2003. https://doi.org/10.1016/j.bbagen.2014.01.007

Hall, B. K. (2005). *Bones and cartilage: developmental skeletal biology* (p. 792). Amsterdam: Elsevier.

Harris, N. L., Rattray, K. R., Tye, C. E., Underhill, T. M., Somerman, M. J., D'Errico, J. A., … Goldberg, H. A. (2000). Functional analysis of bone sialoprotein: Identification of the hydroxyapatite-nucleating and cell-binding domains by recombinant peptide expression and site-directed mutagenesis. *Bone*, *27*, 795–802. https://doi.org/10.1016/S8756-3282(00)00392-6

Hung, P. S., Kuo, Y. C., Chen, H. G., Chiang, H. H., & Lee, O. K. (2013). Detection of osteogenic differentiation by differential mineralized matrix production in mesenchymal stromal cells by Raman spectroscopy. *PLOS One*, *8*, e65438. https://doi.org/10.1371/journal.pone.0065438

Ingram, R. T., Park, Y. K., Clarke, B. L., & Fitzpatrick, L. A. (1994). Age- and gender-related changes in the distribution of osteocalcin in the extracellular matrix of normal male and female bone. Possible involvement of osteocalcin in bone remodeling. *The Journal of Clinical Investigation*, *93*, 989–997. https://doi.org/10.1172/JCI117106

Laizé, V., Martel, P., Viegas, C. S., Price, P. A., & Cancela, M. L. (2005). Evolution of matrix and bone gamma-carboxyglutamic acid proteins in vertebrates. *Journal of Biological Chemistry*, *280*, 26659–26668. https://doi.org/10.1074/jbc.M500257200

Lee, S. J., Baek, S. E., Jang, M. A., & Kim, C. D. (2016). Osteopontin plays a key role in vascular smooth muscle cell proliferation via EGFR-mediated activation of AP-1 and C/EBP beta pathways. *Pharmaceutical Research*, *108*, 1–8. https://doi.org/10.1016/j.phrs.2016.03.041

Liu, Y., Cao, L., Chen, R., Zhou, X., Fan, X., Liang, Y., … Zhao, J. (2015). Osteopontin promotes hepatic progenitor cell expansion and tumorigenicity via activation of b-catenin in mice. *Stem Cells*, *33*, 3569–3580. https://doi.org/10.1002/stem.2072

Mania, V. M., Kallivokas, A. G., Malavaki, C., Asimakopoulou, A. P., Kanakis, J., Theocharis, A. D., … Karamanos, N. K. (2009). A comparative biochemical analysis of glycosaminoglycans and proteoglycans in human orthotopic and heterotopic bone. *IUBMB Life*, *61*, 447–452. https://doi.org/10.1002/iub.167

Morgan, S., Poundarik, A. A., & Vashishth, D. (2015). Do non-collagenous proteins affect skeletal mechanical properties? *Calcified Tissue International*, *97*, 281–291. https://doi.org/10.1007/s00223-015-0016-3

Nadri, S., Soleimani, M., Hosseni, R. H., Massumi, M., Atashi, A., & Izadpanah, R. (2007). An efficient method for isolation of murine bone marrow mesenchymal stem cells. *The International Journal of Developmental Biology*, *51*, 723–729. https://doi.org/10.1387/ijdb.072352ns

Nikel, O., Laurencin, D., McCallum, S. A., Gundberg, C. M., & Vashishth, D. (2013). NMR investigation of the role of osteocalcin and osteopontin at the organic-inorganic interface in bone. *Langmuir*, *29*, 13873–13882. https://doi.org/10.1021/la403203w

Nikel, O., Poundarik, A. A., Bailey, S., & Vashishth, D. (2018). Structural role of osteocalcin and osteopontin in energy dissipation in bone. *Journal of Biomechanics*, *80*, 45–52. https://doi.org/10.1021/la403203w

Papy-Garcia, D., & Albanese, P. (2017). Heparan sulfate proteoglycans as key regulators of the mesenchymal niche of hematopoietic stem cells. *Glycoconjugate Journal*, *34*, 377–391. https://doi.org/10.1007/s10719-017-9773-8

Poundarik, A. A., Boskey, A., Gundberg, C., & Vashishth, D. (2018). Biomolecular regulation, composition and nanoarchitecture of bone mineral. *Scientific Reports*, *8*, 1191. https://doi.org/10.1038/s41598-018-19253-w

Poundarik, A. A., Diab, T., Sroga, G. E., Ural, A., Boskey, A. L., Gundberg, C. M., & Vashishth, D. (2012). Dilatational band formation in bone. *Proceedings of the National Academy of Sciences*, *109*, 19178–19183. https://doi.org/10.1074/pnas.1201513109

Prince, C. W., & Navia, J. M. (1983). Glycosaminoglycan alteration in rat bone due to growth and fluorosis. *Journal of Nutrition*, *113*, 1576–1582. https://doi.org/10.1093/jn/113.8.1576

Rabenstein, M., Hucklenbroich, J., Willuweit, A., Ladwig, A., Fink, G. R., Schroeter, M., … Rueger, M. A. (2015). Osteopontin mediates survival, proliferation and migration of neural stem cells through the chemokine receptor CXCR4. *Stem Cell Research & Therapy*, *6*, 99. https://doi.org/10.1186/s13287-015-0098-x

Ramchandani, D., & Weber, G. F. (2015). Interactions between osteopontin and vascular endothelial growth factor: Implications for cancer. *Biochimica et Biophysica Acta*, *1855*, 202–222. https://doi.org/10.1016/j.bbcan.2015.02.003

Ravindran, S., & George, A. (2014). Multifunctional ECM proteins in bone and teeth. *Experimental Cell Research*, *325*, 148–154. https://doi.org/10.1016/j.yexcr.2014.01.018

Razzouk, S., Brunn, J. C., Qin, C., Tye, C. E., Goldberg, H. A., & Butler, W. T. (2002). Osteopontin posttranslational modifications, possibly phosphorylation, are required for in vitro bone resorption but not osteoclast adhesion. *Bone*, *30*, 40–47. https://doi.org/10.1016/S8756-3282(01)00637-8

Rodriguez, D. E., Thula-Mata, T., Toro, E. J., Yeh, Y. W., Holt, C., Holliday, L. S., & Gower, L. B. (2014). Multifunctional role of osteopontin in directing intrafibrillar mineralization of collagen and activation of osteoclasts. *Acta Biomaterialia*, *10*, 494–507. https://doi.org/10.1016/j.actbio.2013.10.010

Saleh, S., Thompson, D. E., McConkey, J., Murray, P., & Moorehead, R. A. (2016). Osteopontin regulates proliferation, apoptosis, and migration of murine claudin-low mammary tumor cells. *BMC Cancer*, *16*, 359. https://doi.org/10.1186/s12885-016-2396-9

Silva, J. C., Carvalho, M. S., Han, X., Xia, K., Mikael, P. E., Cabral, J. M. S., … Linhardt, R. J. (2019). Compositional and structural analysis of glycosamonoglycans in cell-derived extracellular matrices. *Glycoconjugate Journal*, *36*, 141–154. https://doi.org/10.1007/s10719-019-09858-2

Sroga, G. E., Karim, L., Colón, W., & Vashishth, D. (2011). Biochemical characterization of major bone-matrix proteins using nanoscale-size bone samples and proteomics methodology. *Molecular and Cellular Proteomics*, *10*, M110.006718. https://doi.org/10.1074/mcp.M110.006718

Sroga, G. E., & Vashishth, D. (2018). Phosphoryla tion of extracellular bone matrix proteins and its contribution to bone fragility. *Journal of Bone and Mineral Research*, *33*, 2214–2229. https://doi.org/10.1002/jbmr.3552

Sun, X., Li, L., Overdier, K. H., Ammons, L. A., Douglas, I. S., Burlew, C. C., … Linhardt, R. J. (2015). Analysis of total human urinary glycosaminoglycan disaccharides by liquid chromatography-tandem mass spectrometry. *Analytical Chemistry*, *87*, 6220–6227. https://doi.org/10.1021/acs.analchem.5b00913

Theocharis, A. D., Seidel, C., Borset, M., Dobra, K., Baykov, V., Labropoulou, V., … Hjerpe, A. (2006). Serglycin constitutively secreted by myeloma plasma cells is a potent inhibitor of bone mineralization in vitro. *Journal of Biological Chemistry*, *281*, 35116–35128. https://doi.org/10.1074/jbc.M601061200

Tsao, Y. T., Huang, Y. J., Wu, H. H., Liu, Y. A., Liu, Y. S., & Lee, O. K. (2017). Osteocalcin mediates biomineralization during osteogenic maturation in human mesenchymal stromal cells. *International Journal of Molecular Sciences*, *18*, E159. https://doi.org/10.3390/ijms18010159

Tuck, A. B., Hota, C., Wilson, S. M., & Chambers, A. F. (2003). Osteopontin-induced migration of human mammary epithelial cells involves activation of EGF receptor and multiple signal transduction pathways. *Oncogene*, *22*, 1198–1205. https://doi.org/10.1038/sj.onc.1206209

Vashishth, D. (2007). The role of the collagen matrix in skeletal fragility. *Current Osteoporosis Reports*, *5*, 62–66.

Waddington, R. J., Embery, G., & Last, K. S. (1989). Glycosaminoglycans of human alveolar bone. *Archives of Oral Biology*, *34*, 587–589. https://doi.org/10.1016/0003-9969(89)90100-3

Wang, M., Liu, X., Lyu, Z., Gu, H., Li, D., & Chen, H. (2017). Glycosaminoglycans (GAGs) and GAG mimetics regulate the behavior of stem cell differentiation. *Colloids Surfaces B Biointerfaces. 150*, 175–182. https://doi.org/10.1016/j.colsurfb.2016.11.022

Weber, G. F., Ashkar, S., Glimcher, M. J., & Cantor, H. (1996). Receptor–ligand interaction between CD44 and osteopontin (Eta-1). *Science*, *271*, 509–512. https://doi.org/10.1126/science.271.5248.509

Zoch, M. L., Clemens, T. L., & Riddle, R. C. (2016). New insights into the biology of osteocalcin. *Bone*, *82*, 42–49. https://doi.org/10.1016/j.bone.2015.05.046

SUPPORTING INFORMATION

Additional supporting information may be found online in the Supporting Information section.

How to cite this article: Carvalho MS, Silva JC, Hoff CM, et al. Loss and rescue of osteocalcin and osteopontin modulate osteogenic and angiogenic features of mesenchymal stem/stromal cells. *J Cell Physiol*. 2020;235:7496–7515. https://doi.org/10.1002/jcp.29653